AN ABSTRACT OF THE THESIS OF

Jonathan M. Hatfield for the degree of Master of Science in Mechanical Engineering presented on September 21, 2001. Title: An Exploration of Microcombustor Feasibility.

Redacted for Privacy

Abstract approved: _____

Dr. Richard Peterson

The goals of this research were first to examine flame quenching in tubing smaller than the quench diameter, and then to place lower size limits on microcombustor and microreactor systems by studying a catalytic microcombustor burning propane. In the first set of experiments, flame quenching was examined as a function of wall temperature for various hydrocarbon fuels. This was accomplished by creating a wall temperature profile along a tube, allowing a flame to propagate down the tube, and measuring the temperature of the tube wall coincident with the flame front. This wall quench temperature was plotted as a function of both the equivalence ratio and tube diameter. Fuels tested included propane, hexane, kerosene and diesel. Results showed that quench diameter was reduced by elevating the wall temperature and that the quench temperature increased for increasing mixture flow velocities. Flames were produced in tubes down to 0.8 mm in diameter. In the second set of experiments, a catalyst was used in combination with fuel preheating to obtain a self-sustaining combustion reaction in a chamber approximately 0.25 mm^3 in size. Propane was used in this experiment. Results demonstrated that a stable self-sustaining reaction can be obtained in the microscale regime and that reaction temperatures are on the order of 900°C. This research not only aided in the characterization of hydrocarbon combustion in small diameter channels but also showed promise for development of microcombustor systems.

©Copyright by Jonathan M. Hatfield
September 21, 2001
All Rights Reserved

AN EXPLORATION OF MICROCOMBUSTOR FEASIBILITY

by
Jonathan M. Hatfield

A THESIS

submitted to

Oregon State University

in partial fulfillment of
the requirements for the
degree of

Master of Science

Presented September 21, 2001
Commencement June 2002

Master of Science thesis of Jonathan M. Hatfield presented on September 21, 2001.

APPROVED:

Redacted for Privacy

Major Professor, representing Mechanical Engineering

Redacted for Privacy

Chair of Department of Mechanical Engineering

Redacted for Privacy

Dean of Graduate School

I understand that my thesis will become part of the permanent collection of Oregon State University libraries. My signature below authorizes release of my thesis to any reader upon request.

Redacted for Privacy

Jonathan M. Hatfield, Author

ACKNOWLEDGEMENTS

The author would like to dedicate this research to his wife, Betsy, whose emotional, physical, and spiritual support helped get him through the long hours in the lab. The author would also like to express his appreciation to Dr. Richard Peterson whose guidance helped to make this research a success. For providing technical support in development of the thermal model, the author would like to thank Dr. Murty Kanury. For providing technical support in data analysis, the author would like to thank Dr. Deborah Pence. Finally, for the financial support required to complete this research, the author would like to thank DARPA and PNNL.

TABLE OF CONTENTS

LIST OF FIGURES

LIST OF APPENDICES

LIST OF APPENDIX FIGURES

LIST OF NOMENCLATURE

c_p	Specific heat (J/kg K)
d	Tube diameter (m)
d_Q	Quench diameter (m)
E	Activation energy (kJ/kmol)
h	Convective heat transfer coefficient (W/m^2 K)
k	Thermal conductivity (W/m K)
Nu	Nusselt number
p	Pressure (Pa)
Pe	Peclet number
q_{conv}	Convective heat loss rate (W)
q_{gen}	Heat generation rate (W)
q_{loss}	Flame front heat loss rate (W)
R	Universal gas constant (kJ/kmol K)
S_u	Flame speed (m/s)
S_u^a	Adiabatic flame speed (m/s)
T_f	Flame temperature (K)
T_f^a	Adiabatic flame temperature (K)
T_u	Unburnt mixture temperature (K)
δ	Reaction zone thickness (m)
ϕ	Equivalence ratio
ρ	Density (kg/m^3)

AN EXPLORATION OF MICROCOMBUSTOR FEASIBILITY

1 INTRODUCTION

Combustion processes play an important role in modern society. Today, combustion systems provide power throughout our daily lives from transportation to lawn care. New technological developments are calling for miniaturization of combustion-based power production. To date, little is known about the behavior of combustion systems in the microscale regime. What makes this area attractive is the energy density of hydrocarbon-based fuels: stored liquid fuels when burned with oxygen from the atmosphere have several times the energy density of today's alkaline batteries. In fact, this energy density is on the order of 50 kJ/gm, while that of a conventional AA battery is less than 1 kJ/g. Because of this, it is of great interest to study the feasibility of developing microscale combustion systems for possible battery replacement. The goal of this research is to investigate the behavior of combustion reactions in the microscale regime and determine the feasibility of developing a self-sustaining microcombustor.

To accomplish this, a basic understanding of combustion in the microscale size regime must be acquired. A number of experimental challenges exist in the miniaturization of combustion reactions. First, quenching mechanisms are complex and certain aspects are not completely understood. Second, a quench distance exists that describes a minimum characteristic size through which a flame will propagate. This quenching distance is a function of pressure and temperature. Third, fuel composition affects system behavior in combustion applications. Of particular interest in this research are hydrocarbon fuels, specifically propane, hexane, kerosene and diesel.

The pages herein describe the development of two experiments that pertain to current microscale combustion research. First, a thermal model will be developed that will describe the behavior of combustion reactions in the microscale regime. Second, data will be collected from two experiments and compared to the theoretical model. The first experiment will help characterize the behavior of flames in small diameter quartz tubing. This will be accomplished by varying the tube wall temperature, mixture air/fuel ratio, tube diameter, and fuel type. The response of a propagating flame will be examined and characterized on two graphs, quench temperature vs. stoichiometry and quench temperature vs. quench diameter.

The second experiment will indicate the feasibility of microcombustor development. This will be accomplished using a platinum catalyzed surface reaction and by continued miniaturization of the test apparatus. Third, suggestions will be made pertaining to further exploration into the area of microcombustor development.

2 BACKGROUND

The research described herein is a continuation of existing research in the area of microscale combustion. The following discussion will thus be made up of a description of relevant combustion properties, a discussion of existing microscale combustion research, and the development of a thermal model.

2.1 Flames and Quenching

Combustion is defined as the oxidation of a fuel via chemical reactions with the concomitant release of thermal energy. During this process, a complex set of inter-dependent chemical reactions result in fuel molecules being oxidized. This reorganization of atoms releases energy in two forms: heat and light. The majority of the energy released from the reaction is in the form of heat. This conversion of energy from chemical form to heat is of particular interest because of the high energy density of liquid hydrocarbon fuels.

One major phenomenon of concern regarding combustion in the microscale regime is that of flame quenching. Quenching is said to have occurred when a flame is unable to propagate through a combustible mixture. There are two mechanisms that affect flame quenching. These are heat transfer from the flame front to the surroundings and diffusion of active species. For combustion in tubes, a change in tube diameter causes a change in the surface area-to-volume ratio and thus changes the heat loss from the flame front. This change in surface area-to-volume ratio also affects the number of collisions of active species that are destroyed at the wall. A quantity known as the quench diameter is used to characterize this phenomenon and is defined as the minimum tube diameter through which a flame will propagate at a particular tube wall temperature and gas pressure. It is usually determined experimentally by the following. A flame is established at the opening of a port and the fuel supply suddenly closed. If the flame propagates into the opening, a smaller opening is tested in the same manner. The test is repeated until the flame will no longer propagate into the end of the tube. This becomes the quench diameter.[1] There are several properties of the test system that are shown to affect this quantity. Of particular interest in this research are temperature effects.

Pressure has an inverse effect on quench distance. That is, the higher the pressure, the smaller the tube through which a flame can propagate. For hydrocarbon fuels, this relation is $d_Q \propto P^{-1.2}$. Temperature affects quench distance via mixture preheating and heat loss from the flame front. Mixture preheating decreases the quench diameter by increasing the adiabatic flame temperature. Wall temperature affects the quench distance by modifying the heat loss from the flame. Increasing wall temperature reduces heat loss from the flame front to the wall and reduces the quench distance.[3] This can be seen in Fig. 2.1 taken from Glassman.[1] Temperature effects will be discussed in greater detail later in this chapter.

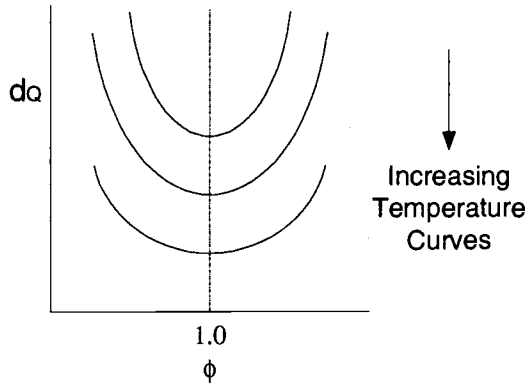

Figure 2.1. Wall temperature effect on quench diameter

Mixture composition is also pertinent in this research. In order to attain combustion, the air/fuel ratio must be within a particular range, called the range of flammability. That is, the air and fuel must be mixed in proportions that allow for oxidation of the fuel. The air/fuel ratio can be calculated by examining the reaction equation. The following describes complete burning of hydrocarbon fuels

$$C_X H_Y + a \cdot (O_2 + 3.76 \cdot N_2) \rightarrow b \cdot CO_2 + c \cdot H_2O + d \cdot N_2 \qquad (1)$$

where C_XH_Y is dependent on the type of hydrocarbon examined and the coefficients a, b, c, and d depend on the amount of air in the reaction. Stoichiometric air/fuel ratio can then be calculated by equating the number of atoms of each element and dividing the amount of reactant air by the amount of reactant fuel. This can be written on either a molar (volume) or a

mass basis. The equivalence ratio (Φ) is often used to define the degree to which a mixture is rich or lean and is defined as the theoretical A/F divided by the actual A/F ratio. Equivalence ratios greater than unity indicate rich mixtures and less than unity indicate lean mixtures.

2.2 Existing Research

Because interest in microscale combustion as a potential power source is a fairly new concept, there is little research that has been done directly on miniaturization of combustion and the problems that exist with such an endeavor. Lucht and Maris[4] show by experimentation that the quench distance decreases as wall temperature increases in internal combustion engines. This demonstrated the relationship between wall temperature and quenching distance as described above.

Zamashchikov[5] has demonstrated the propagation of a stable flame in a preheated stainless steel tube of diameter 2.5 mm. This is below the quench diameter of 3.3 mm for a methane-air mixture at a stoichiometric air/fuel ratio.

Cooley[6] further demonstrated propagation of a stable flame in tubes down to 0.9 mm using a methane-air mixture at a slightly rich mixture ratio (Φ=1.1). He first demonstrated that a flame could be established by preheating the tube walls with a butane burner in a quartz tube of 3.0 mm ID. Once a flame was established in the tube, the wall temperature increased due to heating from the flame, further reducing the heat loss from the flame and allowing the flame to stabilize in the tube. He also demonstrated that as the tube diameter decreased, more tube heating was required to establish a stable flame inside the tube. Cooley further demonstrated that preheating the unburnt gas mixture reduced the quench diameter by increasing the adiabatic flame temperature.

Peterson and Vanderhoff[7] demonstrated experimentally that combustion is attainable at a reaction volume of approximately 0.2 mm^3. This was accomplished using a platinum catalyzed reaction involving hydrogen and air. This research also showed the dependence of reaction temperature on heat loss from the reaction zone. To minimize heat loss Peterson and Vanderhoff isolated the test system in a vacuum chamber, which reduced heat loss by way of convection and conduction.

Sitzki et al.[8] developed microscale excess enthalpy burners fabricated using a process called EFAB. The process can produce arbitrary 3-D structures by stacking hundreds of

individually patterned layers. Using this technique the authors have built and tested both two-dimensional and toroidal versions of their burners that rely on heat recirculation for thermal management. Combustion was attained in a 0.4 mm size channel using a platinum catalyzed surface reaction.

2.3 Thermal Model

The following thermal model is introduced as a theoretical description of thermal reaction limitations. Developed by Mayer[9], this thermal quenching model is a widely accepted theory describing the relationship between flame propagation and heat loss. Mayer begins by defining the heat generation rate as follows

$$q_{gen} \propto \exp\left(\frac{-E}{RT_f}\right) \tag{2}$$

where E is the activation energy and T_f is the flame temperature. From Eq. (2) it can be seen that the generation rate decreases exponentially with flame temperature. Heat loss rates on the other hand can be approximated by a simple temperature difference between the flame and the environment. Mayer explains that this difference in flame temperature dependence results in a limit to which T_f may be reduced (energy balance) before quenching. Figure 2.2 shows how heat loss affects the temperature profile along a flame front.

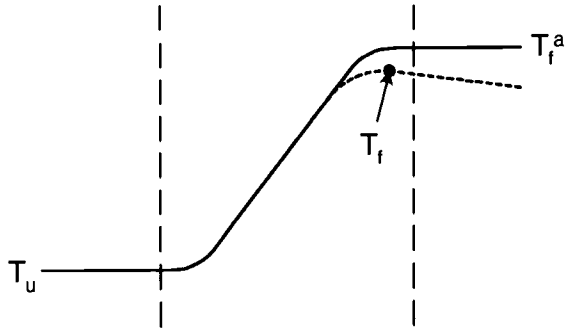

Figure 2.2. Temperature profile along flame with and without heat loss

Mayer then explains critical heat loss mechanisms in terms of two fundamental flame concepts. The first is the representation of the fundamental flame speed in Arrhenius-Semenov form

$$S_u \propto q_{gen} \propto \exp\left(\frac{-E}{RT_f}\right) \tag{3}$$

From the equation it can be seen that as the flame temperature increases, the flame speed increases. The second is the dependence of the reaction zone thickness on the above mentioned fundamental flame speed as follows

$$\delta \cong \frac{\bar{k}}{\bar{\rho} c_{pu} S_u} \tag{4}$$

This equation shows that an increase in flame thickness is produced by a decrease in flame speed. The energy equation is applied assuming heat loss from the flame front by way of convection to the walls of the tube as follows

$$q_{loss} - q_{conv} = 0 \tag{5}$$

where

$$q_{loss} = \rho_u c_{pu} \frac{\pi d^2}{4} S_u (T_f)(T_f{}^a - T_f) \tag{6}$$

and

$$q_{conv} = \bar{h} \pi d \delta (T_f - T_w) = \frac{\pi N u \bar{k}^2}{\bar{\rho} c_{pu} S_u} (T_f - T_w) \tag{7}$$

Subscript u denotes properties evaluated at T_u and the superior bar denotes properties evaluated at an average temperature between T_u and T_f. The quenching diameter is said to be the minimum diameter at which Eq. (5) has a solution.

From the heat loss equation, it is seen that the heat loss rate from the flame front depends on several factors. First, the heat loss from the flame front is dependent on the

cross-sectional area of the flame front. The heat loss rate decreases with flame front cross-sectional area, which is dependent on tube diameter. Second, the heat loss from the flame front is dependent on the flame speed. Increasing the flame speed will increase heat loss and the quench diameter is reduced. Third, the heat loss depends on fuel preheating. This not only affects the temperature at which the properties are evaluated, but also increases the adiabatic flame temperature, which causes an increase in the heat loss term, acting to decrease the quench diameter.

In the convective heat loss rate equation, the properties are also dependent on preheating of the reactant mixture. More notably from Eq. (7) is the dependence of convective heat transfer on the flame front surface area and temperature difference between the flame and the wall. Convective heat transfer is reduced by minimizing the flame front surface area. This can be accomplished by increasing the flame speed, which decreases the reaction zone thickness. Also note that the temperature gradient is defined as the difference between the tube wall temperature and the flame temperature. An increase in the wall temperature reduces the convective heat loss and decreases the quench diameter.

The solution to Eq. (5) can be examined as follows by subsequent rearrangement of terms

$$\left(\frac{\rho_u c_{pu}}{2\bar{k}}\right)^2 \frac{1}{Nu} S_u(T_f)(T_f{}^a - T_f) = \frac{T_f - T_w}{d^2} \tag{8}$$

Figure 2.3 shows curves of the right and left hand sides of the above equation.

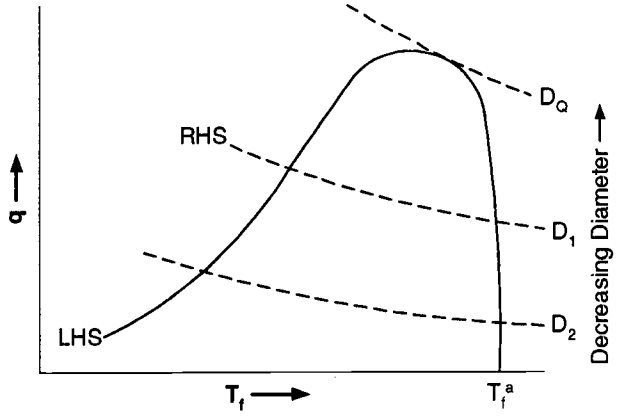

Figure 2.3. Heat loss rate versus flame temperature

From the figure, it can be seen that for relatively large diameters, there exists two solutions to the energy equation. The solution demonstrated on the left side of the heat loss curve is unstable and the solution on the right side of the heat loss curve is stable. As the diameter decreases, the solutions approach each other and a limiting point is reached. This limit is the quenching diameter.

Williams[10] obtains the same result in his analysis of flame quenching due to heat loss. In his analysis, the convective heat loss rate to the surroundings is compared with the heat generation rate of the reaction, as opposed to an estimation of heat loss from the flame front. This ratio of heat generation rate to heat loss rate is generally referred to as the Damköhler number and is said to be on the order of two for ignition in cylinders.[3]

In his analysis of flame quenching, Mayer also mentions the significance of the Peclet number defined as

$$Pe = \frac{S_u{}^a d}{\alpha_u} = \frac{S_u{}^a d \rho_u c_{pu}}{k_u} \tag{9}$$

Experimental results show that the Peclet number is nearly constant for quenching conditions and is on the order of 30-50 for flame quenching of hydrocarbon mixtures. From Mayer's analysis of the Peclet number, compared with correlations of hydrocarbon-air flames, quenching was found to occur at

$$\frac{T_f{}^a - T_f}{T_f{}^a} \approx 0.15 \tag{10}$$

It is important to note that Mayer's analysis was based on using a Nusselt number equal to one.

3 QUENCH TEMPERATURE TEST

Flame quenching characteristics are extremely important when attempting to understand combustion reactions in the microscale regime. As described above, as the tube size decreases, the amount of energy lost by the flame front to the walls increases. Once this energy loss reaches a critical level, combustion cannot be sustained. The following will be a discussion of a system developed to assist in the characterization of flame quenching in small diameter tubes. Comparisons will be made between the experimental results and an approximated analytical solution based on the experimental conditions.

3.1 Experimental Theory

In this set of experiments, a flame was established on the top of a quartz tube of diameter smaller than the quench diameter specified for the fuels to be tested. The tube walls were then heated via an impingement flame and a flame propagated inside the tube. The flame propagated down the tube until it reach a point where the wall temperature was such that there was too much heat loss for a flame to be sustained. A temperature measurement was taken of the tube wall coincident with the meniscus of the flame. Calculations of theoretical wall temperature were made based on the solution to Eq. (5) and subsequent rearrangement of terms as follows

$$T_w = -\frac{\rho_u \bar{\rho} c_{pu}{}^2 S_u{}^2}{4Nu\bar{k}^2}(T_f{}^a - T_f)d^2 + T_f \tag{11}$$

This equation shows the dependence of wall temperature on tube diameter, d, for quenching. From this equation it can be seen that as the tube diameter decreases, a higher wall temperature is required to sustain a reaction. This is in response to the increased convective heat loss resulting from the smaller diameter tube.

3.2 Experimental Apparatus

A schematic of the experimental setup is given in Fig. 3.1. The fuel was supplied by way of a KD Scientific syringe pump. A syringe pump was selected because of its ability to supply small amounts of gaseous and liquid fuels accurately. A glass Hamilton syringe was selected because of its superior dispensing accuracy compared to that of plastic syringes.

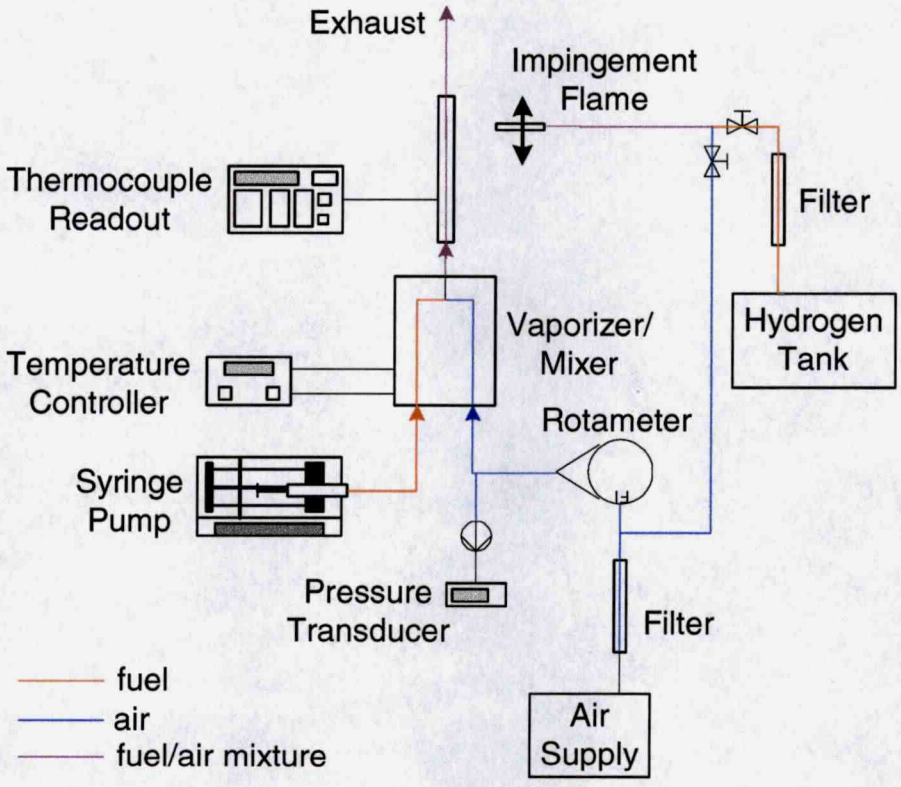

Figure 3.1. Schematic of quench testing setup

Air was supplied from the building line through a filter and controlled by a rotameter. A Validyne pressure transducer, model DP15-42, was placed inline between the rotameter and the vaporizer in order to calibrate the airflow. The range and accuracy of the transducer were 1030 and ± 2.5 torr respectively. Airflow calibration was accomplished using a bubble flow

meter. The pressure in the airline increased with increasing vaporizer temperatures, so the airflow was calibrated at all vaporizer temperature set points.

A fuel vaporizer was designed and constructed for vaporization and mixing purposes. The vaporizer used mica-insulated plate heaters on both sides of the vaporizer in order to provide a uniform temperature throughout. A TEMP-O-TROL temperature controller was used to set the desired temperature of the vaporizer. The sensing thermocouple was embedded approximately 1 cm into the wall of the vaporizer. The setpoint was modified based on the vaporization temperature of the fuel being tested. A viewing window was also constructed to visually inspect the fuel vaporization process. A drawing of the cross-section of the vaporizer assembly and a close-up of the inner concentric tube arrangement can be seen in Fig. 3.2.

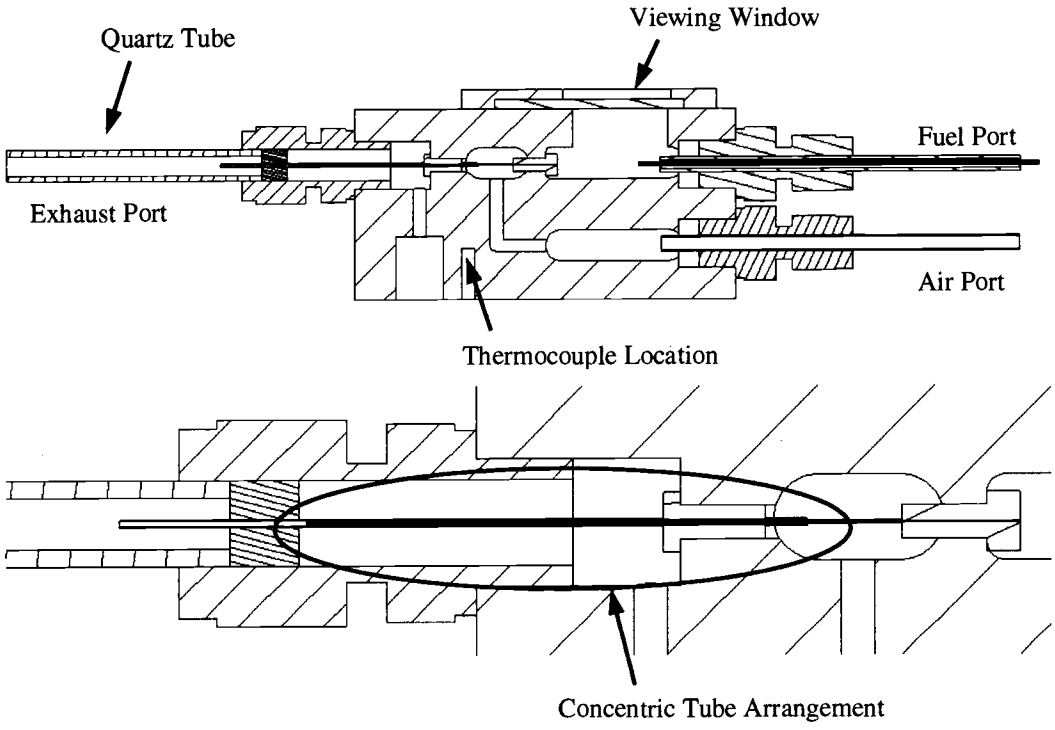

Figure 3.2. Cross-section of vaporizer

A quartz tube was assembled on top of the vaporizer defining the test region for combustion. The tube was prepared by cutting a groove in the wall of a 5 cm quartz tube approximately 2.5 cm from one end. The cut was made perpendicular to the length of the tube and to a depth just breaking through the inner tube wall. This was accomplished by fastening

the tube to a cutting fixture using crystal bond and cutting with a diamond blade wire saw and a 0.01" blade. A type-K, 0.003" diameter thermocouple was embedded in the groove using Omegabond 300 high temperature cement. It was important in this experiment that the thermocouple be placed in good thermal contact with the wall and that it not intrude into the flow. A Keithley thermocouple readout, model 740, was attached to the thermocouple in order to display the measured wall temperature. This readout was selected because of its high sampling rate of eight readings per second. A high sampling rate was necessary because of the dynamic nature of the system. Tube sizes included 2.2, 1.95, 1.10, and 0.8 mm inner diameters.

A hydrogen impingement flame was set up across the tube in order to establish a wall temperature profile streamwise down the tube. Figure 3.3 shows a drawing of the impingement flame setup. The air and hydrogen mixed in the T-section and flowed out the ceramic tip. The air and hydrogen were adjustable using separate valves upstream of the T-section. A flame was generated by first applying a spark to only hydrogen and then introducing air into the flow. The hydrogen and air flow rates were adjusted to provide uniform heating across the tube. The location of the impingement flame was also adjustable along the streamwise direction of the tube by way of a translation stage. Raising and lowering the impingement flame changed the temperature profile along the tube and directly affected the location of the propagating flame inside the tube. This allowed for the location of the propagating flame inside the tube to be positioned so that the appropriate wall temperature measurement could be made.

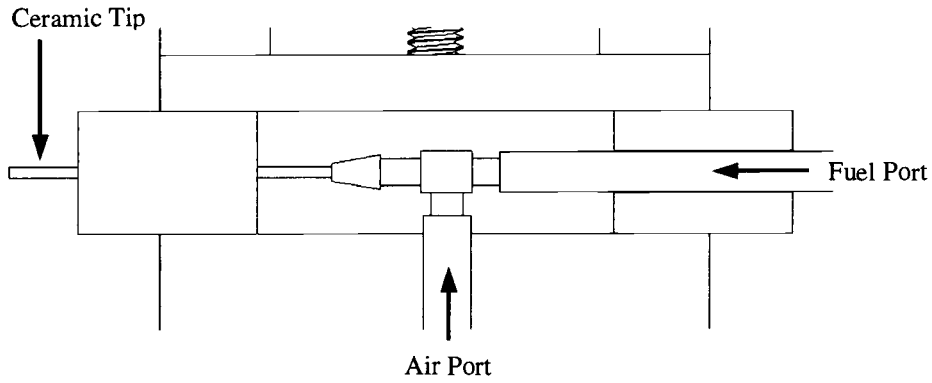

Figure 3.3. Hydrogen Impingement Flame

For testing of fuels with higher vaporization temperatures, a heating coil was placed around the base of the quartz tube between the vaporizer and the thermocouple location. This prevented the fuel/air mixture from condensing after it had exited the vaporizer. The coil was calibrated so that its temperature could be set to match the temperature set point of the vaporizer.

3.3 Experimental Technique

This set of experiments included variations in fuel type, air/fuel mixture ratios, and quartz tube inner diameters. Tests were run first by setting the fuel type and tube diameter, and by varying the air/fuel mixture ratio. Once appropriate data had been collected over a particular range of mixture ratios, a quartz tube of a different inner diameter was assembled onto the vaporizer. Once data had been collected over a range of mixture ratios and tube diameters, the type of fuel was changed.

The objective of this set of experiments was to measure the wall temperature at which a flame will propagate down a tube smaller than the traditional quench diameter. This was made possible by heating the tube, which reduced heat transfer from the flame to the tube walls. The wall temperature is an indicator of how much heat transfer from the flame to the tube wall needs to be reduced in order to sustain a reaction. The fuels tested were propane, hexane, kerosene (assumed tetradecane) and diesel (assumed dodecane) in order of increasing vaporization temperatures. Initially, an attempt was made to keep all mixture flow velocities through the test section constant through all test sets. This was found to be impossible because of the variations in the thermal properties of the tubes, as well as fuel composition and vaporization temperatures. Instead, the fuels were tested initially to determine a flow range for flame stability in each of the tube diameters.

The first step in each set of experiments was to calibrate the airflow rate for the vaporizer temperature set point of the fuel to be tested. For propane, the vaporizer was set at room temperature. For hexane, the vaporizer was set at 80°C. For kerosene and diesel, the vaporizer was set at 240°C. The largest quartz tube was assembled onto the fuel vaporizer for testing and the base sealed using silicon sealant. A flame was produced in the tube and the range of flow velocities producing a stable flame were identified. Once a flame stability range

was determined, two flow velocities were selected as set points at which to collect data. These two flow velocities were set by manipulating the airflow pressure reading.

The flame location along the inside of the tube was adjusted by way of adjusting the location of the impingement flame along the outside of the tube. A temperature measurement was read from the embedded thermocouple when the bottom of the flame meniscus reached the thermocouple level and stabilized. The cross-section of the flame at the time of measurement can be seen in Fig. 3.4. A microscope was placed at eye level with the thermocouple in order to accurately view the flame meniscus. As soon as the flame meniscus reached the top of the groove in which the thermocouple was embedded, the thermocouple readout was observed and a temperature measurement recorded. It was important to note that the repeatability of the experiment was somewhat dependent on the person collecting the data. That is, the test system was small enough and the temperature gradient in the tube great enough that it was essential for the person collecting the data to do so in precisely the same manner every time. This increased the uncertainty in the collected data. Because of this, several measurements were collected to ensure the accuracy of the data and give an indication of experimental uncertainty.

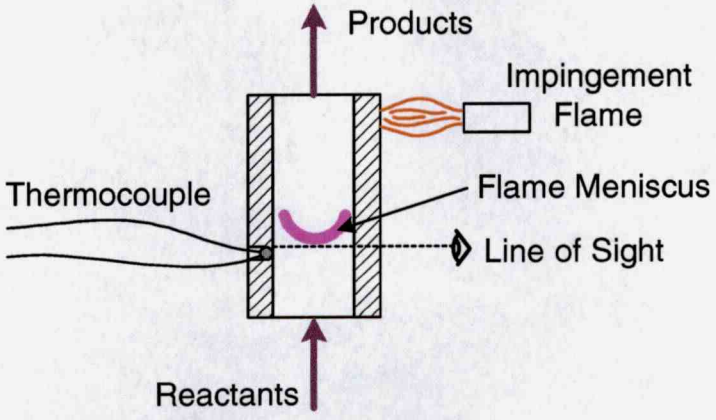

Figure 3.4. Flame location for temperature measurement

To collect a set of wall temperature data, the airflow was set at the low set point, and the fuel flow rate was adjusted such that the air-to-fuel ratio was approximately stoichiometric. The impingement flame was initiated and a stable flame was produced in the

tube. The location of the impingement flame was adjusted and a measurement of the wall temperature coincident with the flame front was collected as described above. Each measurement was repeated three times for a specific mixture ratio to determine the repeatability of the measurement. The fuel flow rate was adjusted and three more measurements taken at a different mixture ratio. This procedure was repeated for the range of equivalence ratios for which a stable flame could be sustained. The airflow rate was increased to the higher set point. The same procedure was used to attain wall temperature data at the higher airflow rate. The system was shut down and allowed to cool. The above procedure was repeated for the same fuel, tube diameter, and air/fuel mixture ratios. Once the second set of data had been collected, the system was allowed to cool, the quartz tube changed and the system reheated to operating temperature. The above procedure was repeated over the range of tube sizes. Once all data had been collected for a given fuel, the fuel was changed and the fuel vaporizer temperature set point adjusted to accommodate the fuel to be tested. The above procedures were followed for the new fuel. This was repeated for all the fuels tested. The above mentioned set of experiments produced two sets of data for each combination of fuel, tube diameter, and equivalence ratio. The wall temperature data was plotted versus equivalence ratio and the minimum temperature values plotted versus quench diameter.

3.4 Experimental Issues

There were several experimental issues to be addressed in this investigation. One such experimental issue pertained to the vaporization of the fuels. This became especially significant when testing diesel. The maximum operating temperature of the vaporizer was believed to be 270°C, beyond which the internal sealing gaskets and O-rings would slowly decompose. Because of diesel's high vaporization temperature and complex structure, not all of the fuel was vaporized. It is believed that the lower boiling point compounds of the fuel were vaporized, which would change the composition of the fuel actually burned. Also at such high vaporization temperatures, the flow within the vaporizer displayed inconsistent behavior. It was found that at elevated temperatures, the concentric tube arrangement shown in Fig. 3.2 produced a flow constriction that affected the air/fuel flow path, and subsequently affecting flame stability. For this reason, the lengths of the stainless steel tubes within the

vaporizer were shortened, which reduced flow resistance and decreased the pressure effects. The vaporizer was recalibrated before testing resumed.

Another such issue was the idea of pressure correction. It was thought that the elevated pressure in the air and fuel lines upstream of the vaporizer would affect the air/fuel mixture composition. Pressure correction provided a way to account for this increased pressure for mixture ratio calculation. Pressure correction was not needed for the airflow rate because the airflow was calibrated based on the test section exit flow rate after the flow constriction. Liquid fuels were assumed to be incompressible and so pressure effects were negligible. Propane was the only fluid requiring pressure correction. There was no pressure tap in the propane line while running the experiment, so the test system was reassembled with a pressure tap in the fuel line and propane and air run to simulate testing conditions. The fuel line pressure was calibrated with fuel volumetric flow rate. This gave an indication of the pressure correction necessary for given fuel flow rates and allowed the pressure effects to be taken into consideration in the calculations of mixture ratio. These effects were shown to be on the order of five percent for propane.

Quartz tube wall thickness also became pertinent in this set of experiments. The purpose of the impingement flame was to heat the walls of the tube uniformly. Since quartz has a relatively low thermal conductivity, increasing the wall thickness created thermal patterns in the cross section of the tube and prevented uniform tube heating. For this reason, the flames produced in the thick walled tubing were somewhat unstable and appeared to hug the walls closest to the impingement flame or at the highest temperature.

3.5 Experimental Results and Discussion

The results of the above set of experiments are given in Figs. 3.5 through 3.8. Quench tests using propane, hexane, kerosene and diesel are shown. All results show an increased wall temperature is required to propagate flames in tubes of decreasing diameters. There is a U-shaped trend in the data indicating a minimum wall temperature for flame propagation. The equivalence ratio coincident with this minimum wall temperature is marginally on the rich side of stoichiometric, which is consistent with the findings of Cooley[6]. For kerosene and diesel, there is also a shift in the minimum wall temperature mixture ratio from right to left as tube diameter is decreased. The assumption of these fuels to be simple hydrocarbon mixtures

may be affecting the stoichiometric air/fuel mixture ratio calculations. For diesel, the wall temperature measurements are shifted significantly to higher equivalence ratios, or rich mixtures. This is due to the incomplete vaporization of the fuel as discussed previously. It is important to note that the equivalence ratio as indicated in the figures is the equivalence ratio as fed into the fuel vaporizer, and not necessarily that as seen by the reaction. The U-shaped trends in the data showing an increasing wall temperature on each side of the minimum wall temperature indicate flammability limits for this particular experimental configuration. Experimentally, as these limits are approached, the wall temperature began to oscillate significantly and the uncertainty in the temperature measurements increased. Also note that for a given tube diameter, increasing the mixture flow velocity caused an increase in the measured wall temperature for quenching. This is believed to be due to the increased convective heat loss from the flame front to the tube wall. A final observation is that for smaller tubes, the U-shaped trend in the data is less pronounced. This is especially true for the 0.8 mm tube diameter where the system demonstrated signs of increased instability.

Figure 3.9 shows the minimum wall quench temperature of each fuel versus the tube inner diameter. The data show an increase in wall temperature required to propagate a flame as the tube diameter decreases for all fuels tested. This tube diameter dependence of wall temperature for quenching is consistent with Eq. (11). No conclusions between the actual temperature values of the different fuels can be made at this point due to the uncertainties in the data pertaining to flow rate considerations and actual temperature measurements.

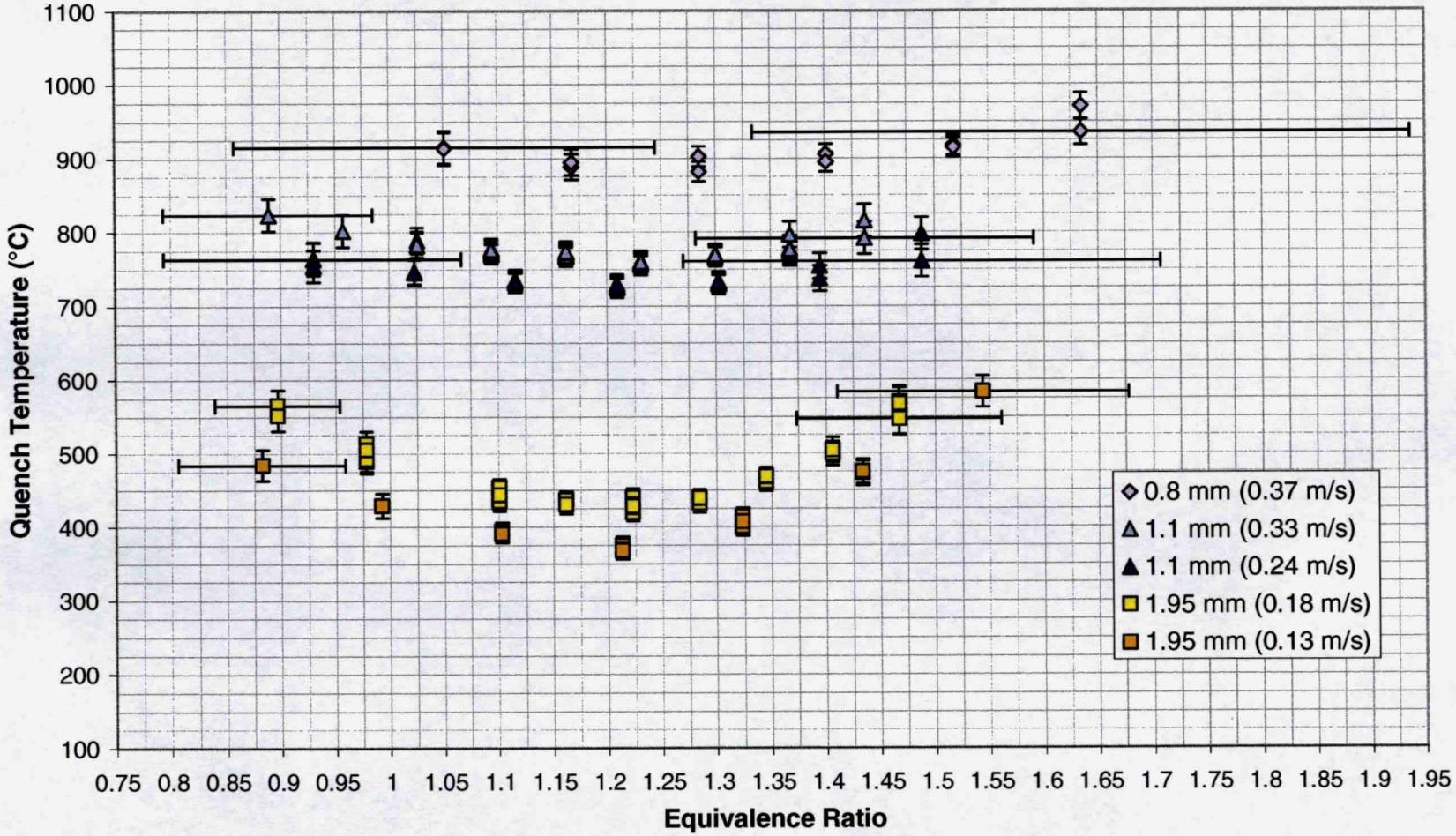

Figure 3.5. Propane quench test results

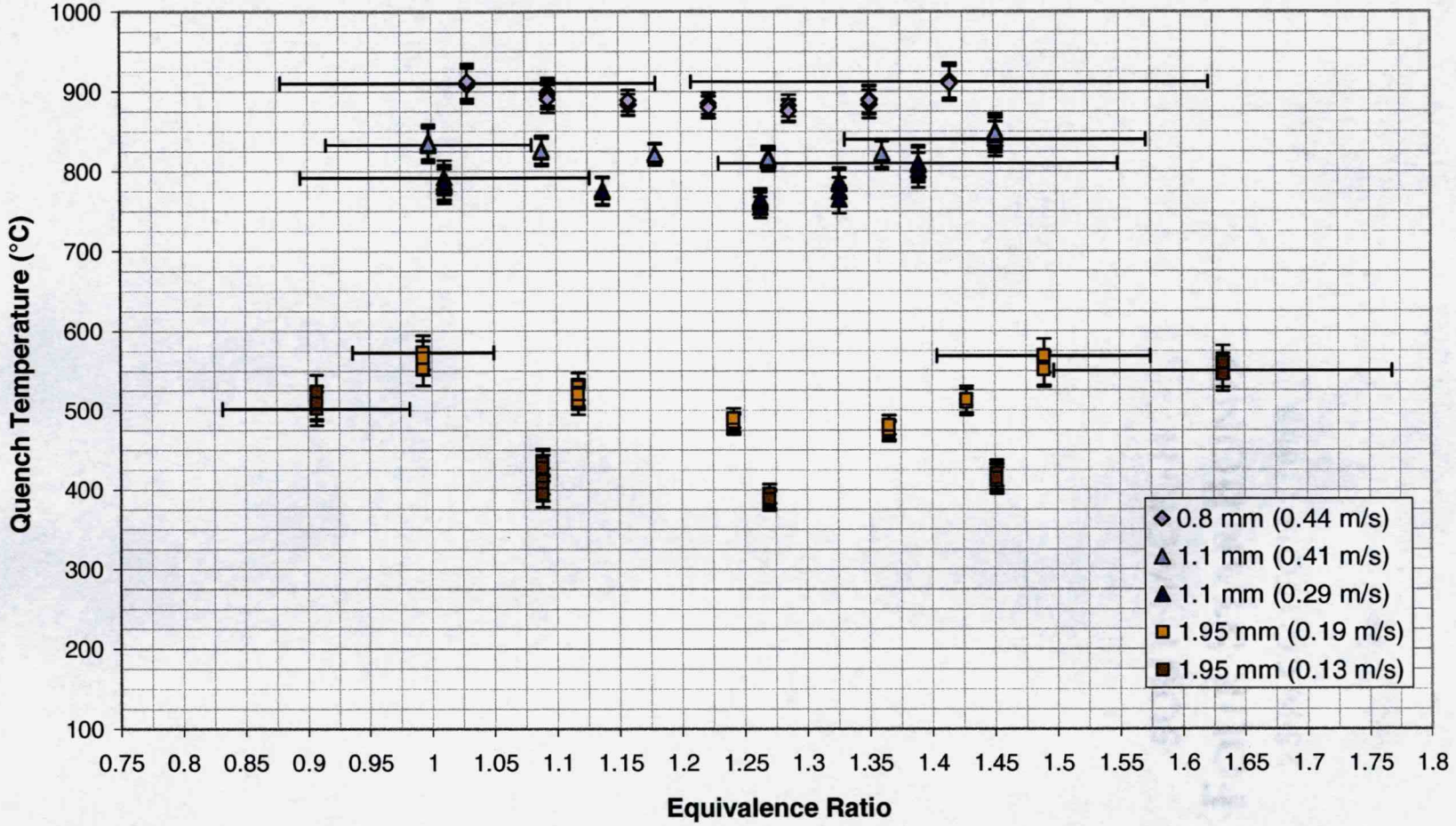

Figure 3.6. Hexane quench test results

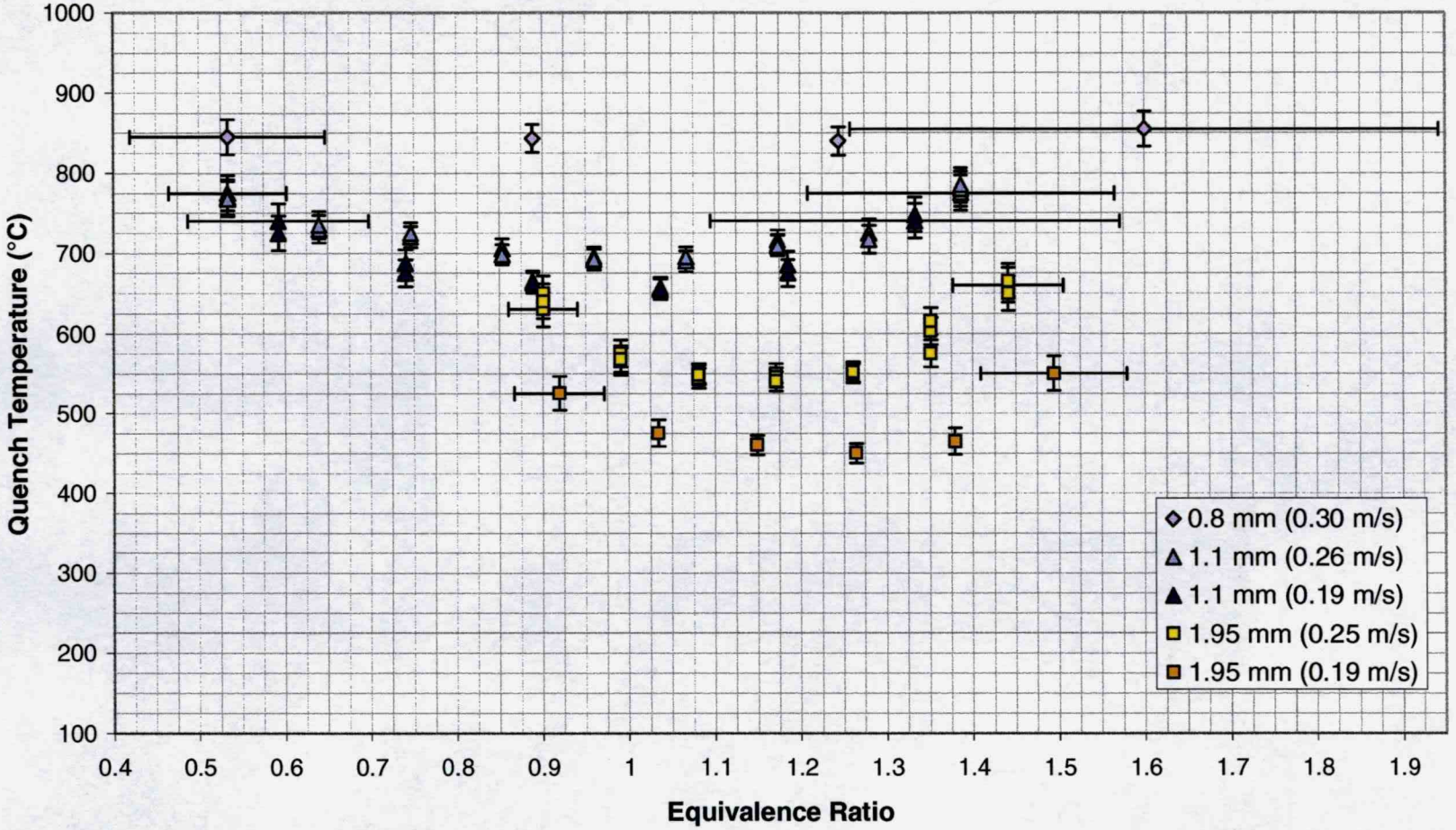

Figure 3.7. Kerosene quench test results

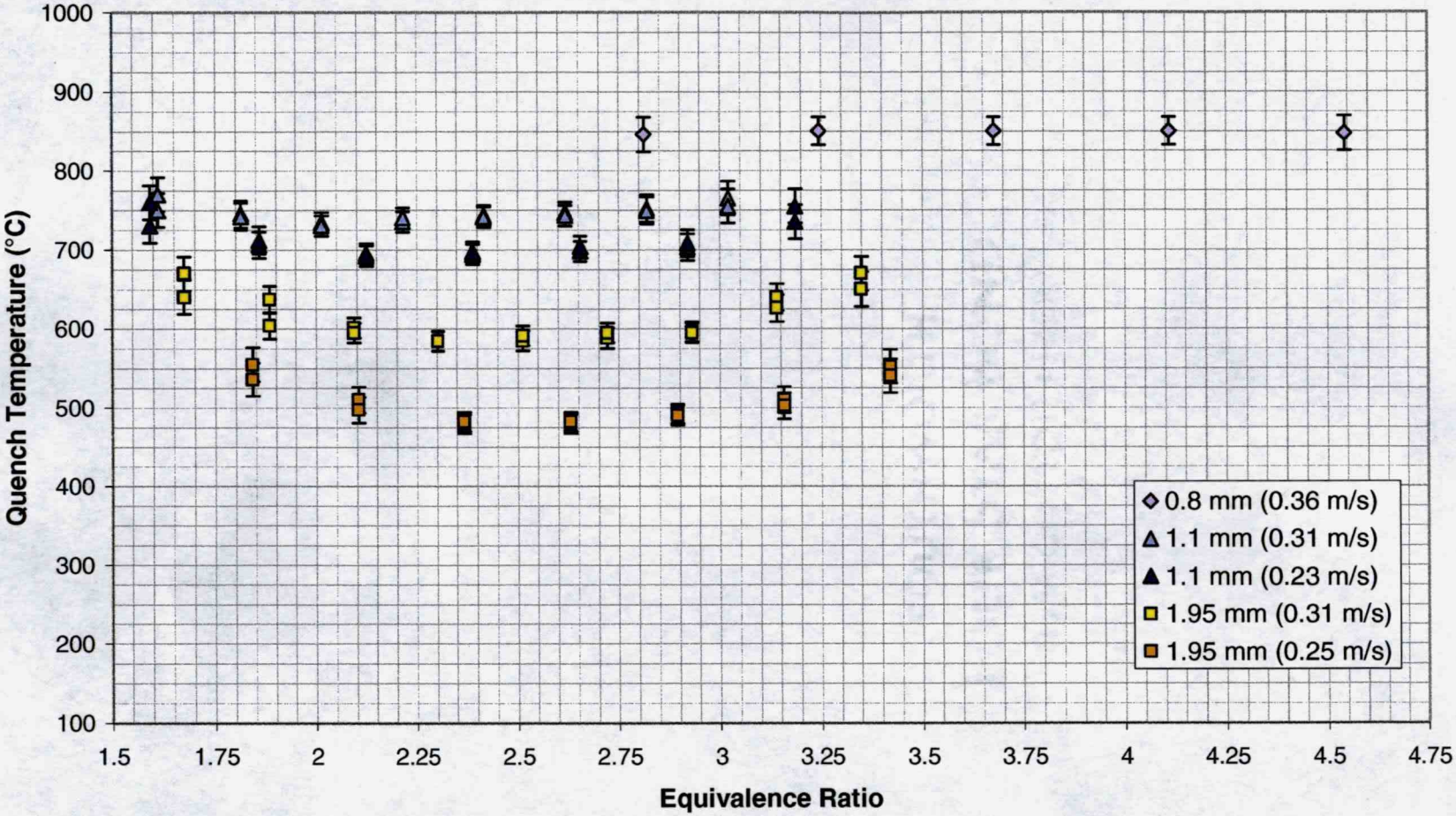

Figure 3.8. Diesel quench test results

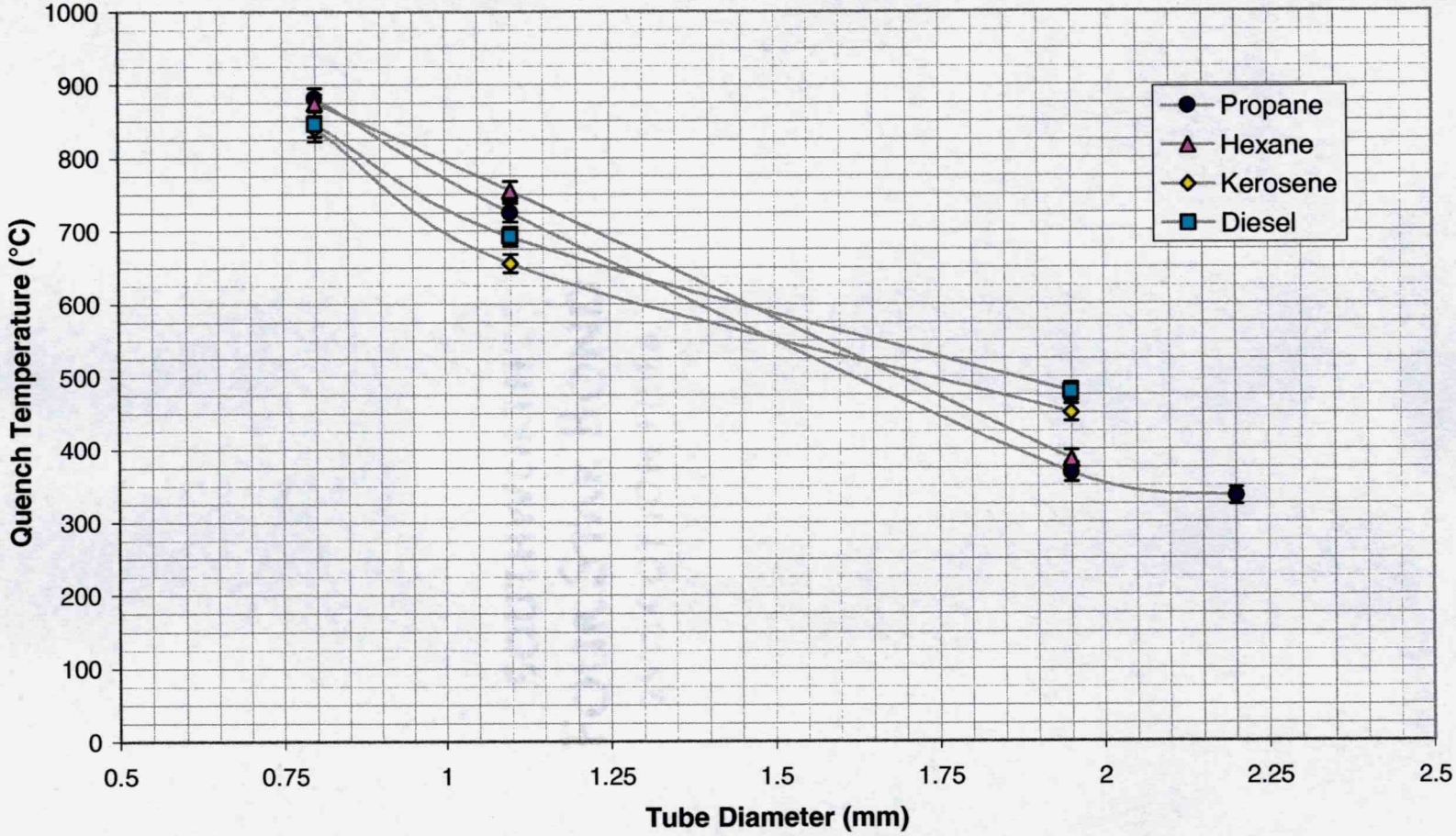

Figure 3.9. Minimum quench temperature vs tube diameter

Calculations were made of the theoretical wall temperature versus quench diameter using Eq. (11) and the experimental conditions. To accomplish this, a thermal model was developed to estimate the temperature of the air/fuel mixture entering the reaction zone. This thermal model was based on the assumption that the temperature profile along the tube was linear between the measured wall temperature and the fuel vaporizer. Knowing the temperature profile along the tube, tube geometry, fluid properties, and fluid inlet temperature allowed for calculation of the fluid exit temperature using an internal flow analysis. This model showed that the temperature of the fluid would closely follow that of the tube for this test configuration. Flame temperature was first calculated using Eq. (10). A Nusselt number equal to 4.0 was used in this calculation based on an approximation for heat transfer in circular tubes. The results of this calculation for propane and hexane can be seen in Figs. 3.10 and 3.11, respectively. Calculations for kerosene and diesel could not be made due to a lack of fuel property information. Thermo-physical properties for propane and hexane were obtained from Brigham Young Chemical Engineering Thermophysical Property Database.[11] Combustion properties were calculated from thermodynamic properties obtained from CRC.[12]

Results show significant differences between the theoretical values and the measured values. Discrepancies are believed to be due to a few contributors. First, calculations were made using T_f approximated from Eq. (10). This approximation assumes that T_f at quenching is independent of tube size and flame speed. As the tube diameter decreases, the heat loss from the flame will increase and so flame temperature will decrease. Second, in this experiment a stable flame was produced inside the tube. This flame acts to heat up the tube wall, which reduces heat loss from the flame front to the tube wall and further reduces the quench distance. Also affecting the quench diameter are the mixture preheating effects caused by conduction of the heat generated by the flame down the tube walls. Third, in Mayer's analysis a Nusselt number of one was used, as opposed to using a Nusselt number of 4.0 as approximated for heat transfer in circular tubes.[13] Of significant interest is the effect of flame speed on the wall temperature. Flame speed was estimated by calculating the flow velocity of the unburnt mixture just prior to entering the reaction zone. Measured wall temperature values increased with increasing flame speed while calculated wall temperature values decreased with increasing flame speed. The calculated value for propane at a diameter of 2.2 mm is significantly decreased from that of 1.95 mm. This is believed to be due to the fact that the diameter is approaching the quench diameter.

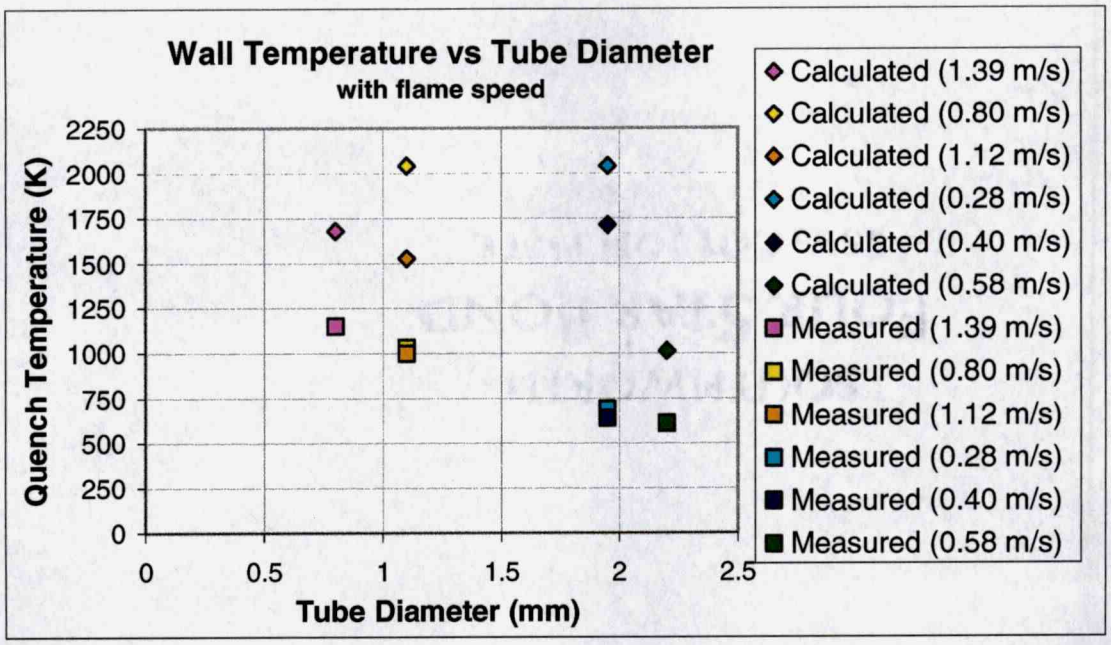

Figure 3.10. Comparison between theoretical and measured quench temperature values as dependent on quench diameter and flame speed (propane)

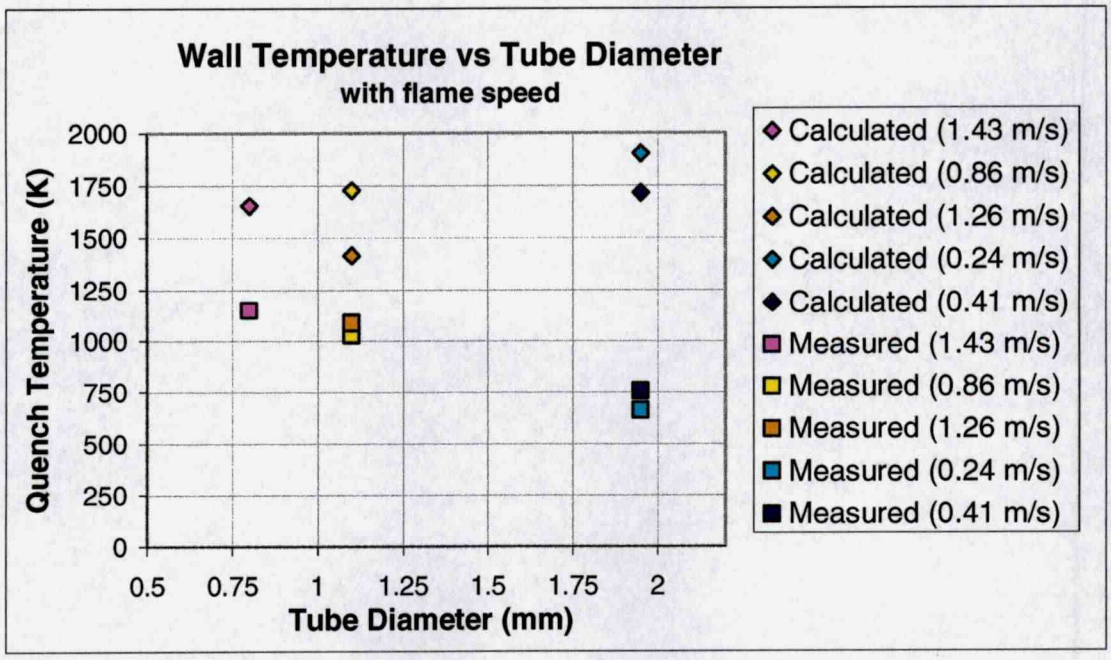

Figure 3.11. Comparison between theoretical and measured quench temperature values as dependent on quench diameter and flame speed (hexane)

Figures 3.12 and 3.13 show flame temperatures calculated by rearranging Eq. (11) based on the wall temperatures measured in the experiment. The figures show that the calculated flame temperature is not constant for quenching, but is dependent on the tube diameter and mixture flow rate. The figures indicate that flame temperature increases with flame speed for a given tube diameter. Also, it appears that flame temperature increases with tube diameter for a given flame speed. More tests need to be done in order quantify this conclusion.

3.6 Uncertainty Analysis

Uncertainty was calculated using the Kline-McClintock[14] method. In this analysis, all sources of uncertainty are combined to indicate total uncertainty in a quantity. In this set of experiments, measured temperature and mixture composition require estimations of uncertainty.

There were two major contributors to uncertainty in the temperature data. The first was uncertainty associated with how accurately the temperature could be read from the temperature readout. This included estimations of visibility of the flame front as well as measurement repeatability. It was found that the data could only be collected within a range of uncertainty of ±10°C for mixtures near stoichiometric and ±20°C for those near the flammability limits. The second was uncertainty due to the instrumentation. The uncertainty associated with the thermocouple included many considerations. Most easily accounted for was the specified uncertainty for the type of thermocouple used. Other considerations included thermocouple placement and mode of heat transfer. In this research, the thermocouple was embedded into the wall via high temperature cement. A thermal model was developed to ensure that the radiation from the flame did not significantly affect the temperature measurement. The thermal model also gave an indication as to the response time of the thermocouple. The analysis showed that radiation effects were insignificant and that the response time of the thermocouple was sufficiently fast due to its being in direct thermal contact with the wall. The uncertainty due to the thermocouple readout was based on the sampling rate, the specified uncertainty and the resolution. Estimating a temperature ramp and dividing that ramp by the sampling rate allowed for calculation of the uncertainty due to the sampling rate. It was calculated that the most significant factor to the uncertainty in the

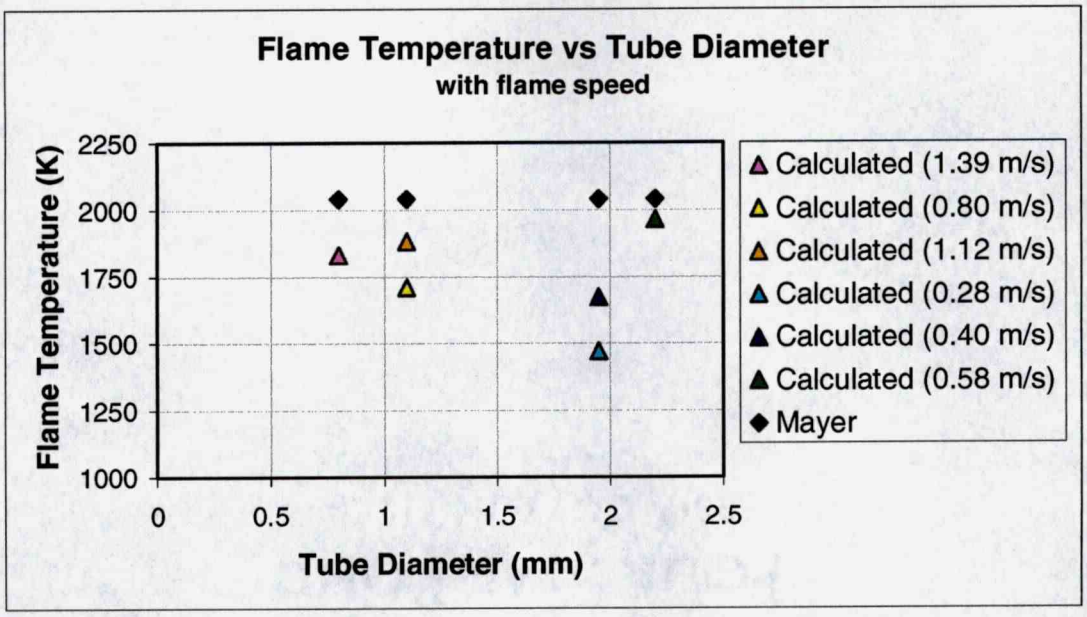

Figure 3.12. Comparison between Mayer's theoretical flame temperature and calculated flame temperature at quenching (propane)

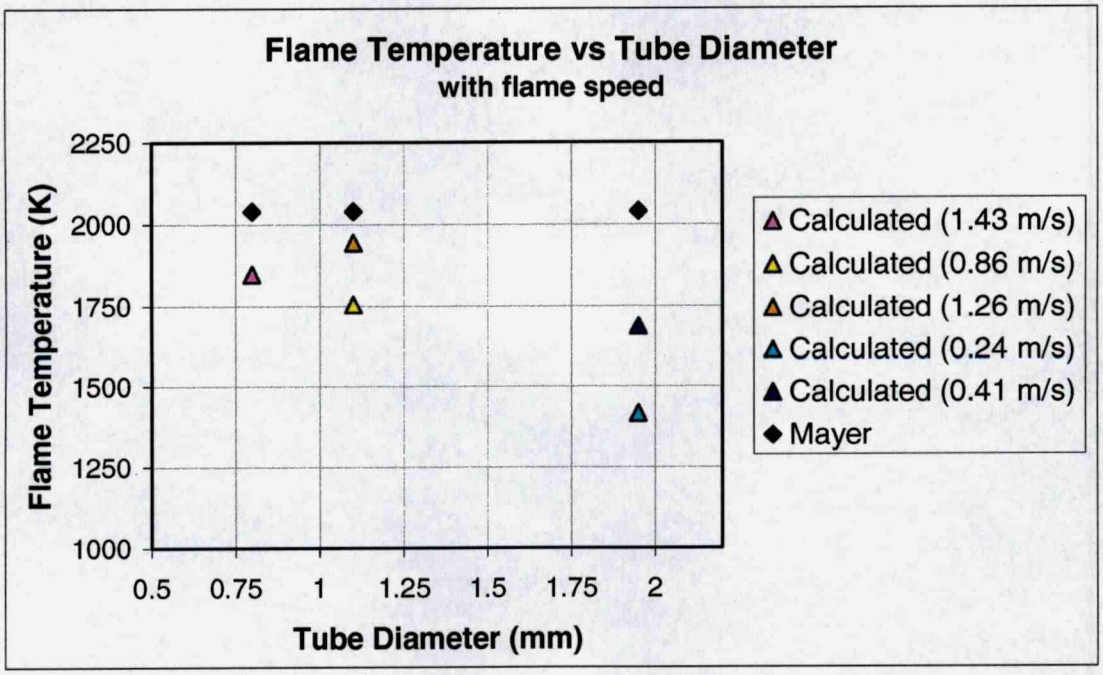

Figure 3.13. Comparison between Mayer's theoretical flame temperature and calculated flame temperature at quenching (hexane)

temperature measurement was the human factor in collecting the temperature data. At higher temperatures, the specified uncertainty in the thermocouple also played a significant role. The values of uncertainty ranged from ±12°C near stoichiometric mixtures to ±25°C at rich and lean mixtures.

There were also two major contributors to the uncertainty in mixture composition. The first was uncertainty due to the air/fuel supply. This proved to be complex due to the method of air feed. The calibration of the airflow rate with pressure via a bubble flow meter was believed to be a significant factor in calculation of uncertainty. The effects of the bubble flow meter and stopwatch resolutions were determined, the vaporizer temperature effects considered, and uncertainties due to pressure transducer readings estimated. Vaporizer temperature and pressure transducer effects were determined from a calibration chart. Also important to consider here is uncertainty due to human factor. To account for this, each calibration measurement was taken three times to determine repeatability and indicate uncertainty. The fuel flow uncertainty was determined by the specified uncertainty of the syringe pump and the type of syringe used. A second contributor to uncertainty taken into consideration for diesel fuel testing was that of the unvaporized fuel. This value could not be estimated to any degree of certainty and so error bars do not appear in Fig. 3.8. For propane, pressure correction also contributed to uncertainty. The major contributors to uncertainty in the mixture composition were the effects of vaporizer temperature and pressure variation on reading the calibration chart for airflow. Uncertainty of the equivalence ratio was calculated to be as much as ±0.25 for low flow rates and as low as ±0.03 for high flow rates.

4 MICROCOMBUSTOR TEST

Studying microcombustor feasibility was the second goal of this research. As described previously, as the size of the combustion chamber is reduced, heat loss from the reaction front to the walls of the chamber increases. This creates a quench limit giving the minimum size in which a flame can be sustained. For this reason, it becomes more and more difficult to attain a self-sustaining combustion reaction as the combustion chamber size is reduced. The following will be a discussion of an experiment designed to examine a self-sustaining catalytic microcombustor. Reaction zone temperature will be plotted against equivalence ratio for a range of fuel flow rates.

4.1 Experimental Theory

One of the goals of this investigation was to reduce the size of a combustion chamber to one cubic millimeter or less while sustaining a combustion reaction. Several mechanisms were used to aid in both the initiation and sustaining of a reaction in such small volumes. As mentioned in the previous chapter, quenching will come in the form of free radical destruction at the wall of the combustor and in the form of heat loss to the surrounding structure. First, consideration of radical destruction leads to the idea of employing a heterogeneous catalytic surface to promote reactions rather than hinder them. In this set of experiments, platinum was used as the catalyst. Second, recirculation of the exhaust gases was used to preheat the reactant mixture in a counterflow heat exchanger arrangement. This preheating increases the adiabatic flame temperature of the reaction, further decreasing the quench diameter by Eq. (11). Third, quartz tubing was used for the walls of the chamber. This reduced the heat loss through the walls of the combustion chamber by reducing the wall thermal conductivity. Also of significance here is the high melting point of quartz, which prevented the system from failing at elevated temperatures. It was theorized that a combination of these effects would be enough to counteract quenching effects in very small chambers resulting in combustion in chambers significantly smaller than the characteristic quench distance. In this set of tests, propane (C_3H_8) was used.

4.2 Experimental Apparatus

A schematic of the experimental set-up is given in Fig. 4.1.

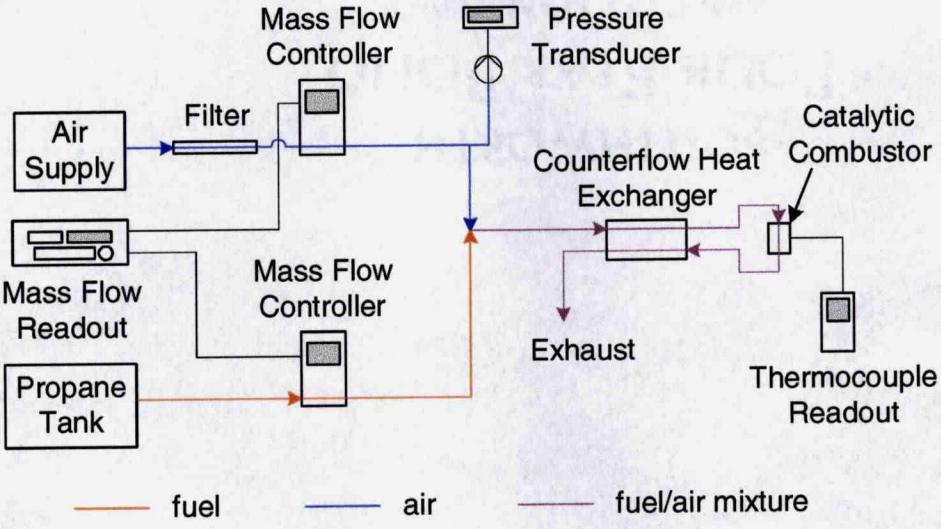

Figure 4.1. Schematic of catalytic microcombustor test setup

The fuel was supplied by way of an MKS mass flow controller, model M100B11CP1BV, from a propane tank. The decision to use flow controllers was made because of pressure variations caused by the reduced size of the combustion chamber. These effects will be discussed later. To measure the mass flow rate, the controller applies a specified heat flux to the flow passing through the device and measures the temperature on both sides of the flux. The device uses the thermal energy change equation $Q = \dot{m} c_p \Delta T$ to calculate the mass flow rate of a specific gas with a known c_p.

Air was also supplied via an MKS mass flow controller, model M100B12CP1BV, but from the building line through an air filter. Since the air flow rate was supplied at higher levels than the fuel, a flow controller with a larger range was used. A Validyne pressure transducer, model DP15-42, was placed in the airline near the mixing section to monitor the inlet pressure to the combustor. The range and accuracy of the transducer were 1030 ± 2.5 torr, respectively. Fuel and air were mixed at a T-section in the line.

The counterflow heat exchanger and combustion chamber were assembled as follows. The counterflow heat exchanger was created by epoxying a 27-gauge stainless steel tube into a T-section tube fitting such that one end projected out approximately 5 cm. This allowed the other end of the stainless steel tube to be attached to the inlet tubing. A quartz envelope could then be slipped over the top of the stainless steel tube to define the flow path. The inlet gas travels straight through the T-section inside the SS tubing until it reaches the end of the quartz envelope, at which point the flow is forced back around the outside of the SS tubing to exit out the side port of the T-section. Figure 4.2 shows a cross section of the counterflow heat exchanger/combustor system.

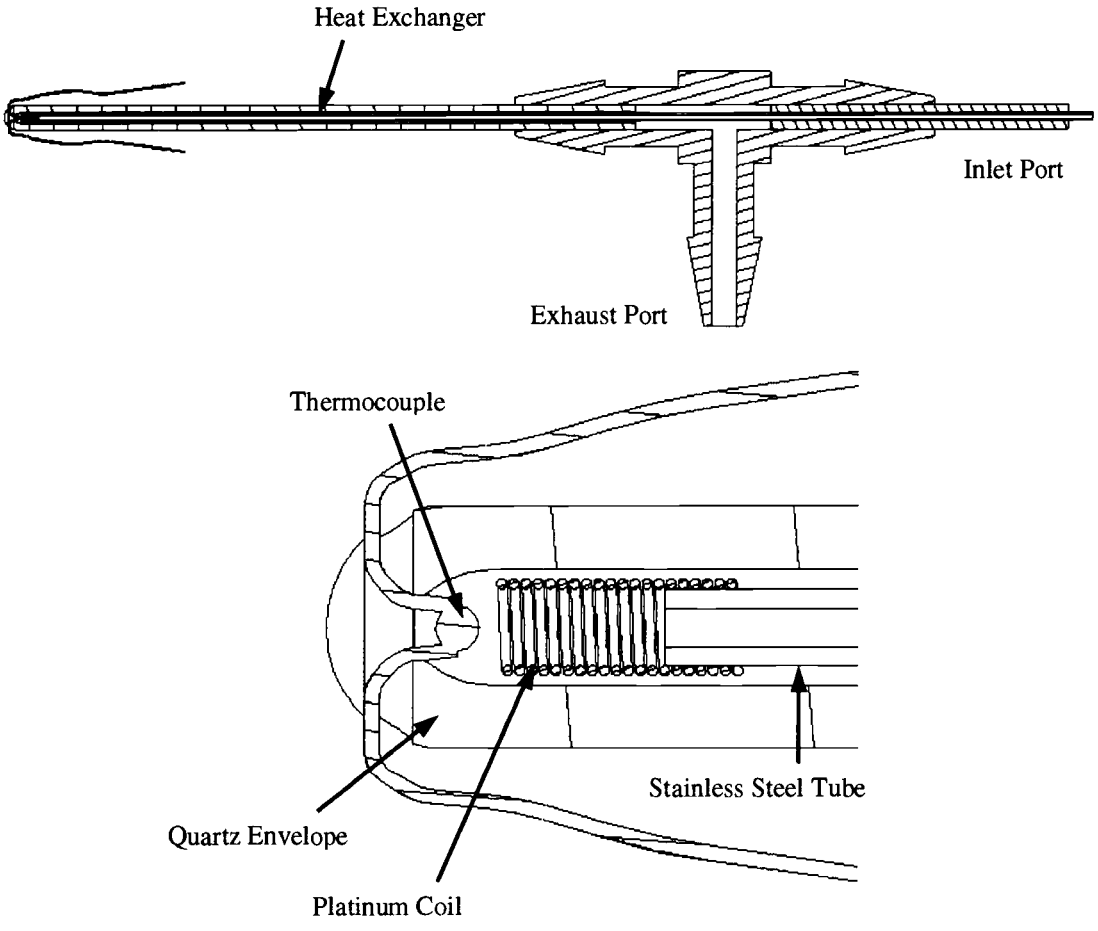

Figure 4.2. Cross-section of the microcombustor test assembly

The combustion chamber was next constructed in two steps. First, the platinum coil was prepared by wrapping 50 micron platinum wire around the SS tubing and pushing approximately one millimeter of the coil off the end of the SS tubing. The Quartz envelope was prepared by fastening a thermocouple to the end after closing via an acetylene torch. A slot was cut in the tip of the closed end perpendicular to the length of the tube such that a small opening was produced in the tip. This was accomplished by fastening the tube to a cutting fixture using crystal bond and cutting with a diamond blade wire saw and a 0.01" blade. A 0.003" type-K thermocouple was inserted into the opening and cemented into place using Omegabond 300. The thermocouple leads were shrink-wrapped along the outside of the quartz envelope. A Tektronix thermocouple readout, model DTM920, was attached to the thermocouple leads to attain a temperature measurement of the reaction zone. The prepared quartz envelope was slid over the top of the SS tube/platinum coil assembly and sealed using silicon. A close-up of the prepared reaction zone can be seen in Fig. 4.2.

A removable coil was constructed by wrapping heating wire around the outside of a three millimeter quartz tube and bending the wire ends to create leads in order to attach the coil to a power supply. The heating coil was placed over the closed end of the quartz envelope in order to heat the platinum surface to initiate a reaction. Also a Plexiglas shield was cut and placed around the test system to reduce the convective heat transfer effects of air circulation in the room.

4.3 Experimental Technique

The goal of this set of experiments was to develop a microcombustor system capable of a self-sustaining combustion reaction in a chamber smaller than one cubic millimeter. A propane/air mixture was used in this set of tests. Setting the mixture ratio to stoichiometric and heating the combustion region generated the surface reaction initially. The heat source was then removed and the reaction allowed to stabilize. Stability of reaction was determined by the settling of the reaction zone temperature measured by the embedded thermocouple. Once a stable reaction was produced, the fuel and airflow rates were slowly adjusted to the desired values so as to not disturb the stability of the reaction. The fuel flow rate set points were 0.5, 1.0, 1.5, 2.0 and 2.5 sccm of propane. The air was set so that the air/fuel ratio was at stoichiometric, the system allowed to stabilize and a temperature measurement recorded. The

airflow was reduced incrementally, each time allowing the reaction to stabilize. This was repeated until the combustion process became significantly unstable. The airflow was adjusted back to stoichiometric and the reaction initiated via the heating coil. Once combustion was attained, the heating coil was removed and a temperature was recorded upon settling of the system. The airflow was increased incrementally, each time allowing the reaction to stabilize. This was repeated until the combustion process became significantly unstable, this time at the lean mixture limit. This procedure was repeated for all fuel flow rates providing two sets of data for each.

The test system was also disassembled and examined for oxidation and corrosion. There appeared to be a significant amount of oxidation damage in the hot end of the system due to the elevated temperature at which the system operates. It was found that limiting the reaction temperature to 900°C and flushing the system with air until all moisture was removed minimized the damage to the SS delivery tube. Future experiments should employ SS tubes with an alloy having greater high temperature resistance than 303 or 304.

4.4 Experimental Issues

There were several experimental issues to be investigated in this portion of the research. One such issue was the ignition of the reaction. It was found to be very difficult to ignite the surface catalytic reaction in the chamber if not burned in the atmosphere first. This indicates that a necessary surface preparation is needed in order to facilitate thermal ignition. Surface preparation in this research consisted of producing a surface reaction in the atmosphere via a flame before inserting the coil assembly into the quartz envelope and attempting thermal ignition.

Thermocouple location was also an important issue to be considered; first in fastening of the thermocouple to the quartz envelope and then in its placement. The fastening of the thermocouple was of concern because of the high temperatures at which the system operated. Omegabond 300 was operable at the elevated temperatures, but its thermal expansion was different enough from that of quartz that separation occurred. For this reason, a thermocouple-embedding scheme, as described previously, was developed and implemented to remove thermal expansion effects. Thermocouple placement was important in that the desired temperature to be measured was the temperature of the reaction zone. To accomplish

this, the thermocouple was placed inside the tip of the quartz envelope near the reaction zone. One concern with this thermocouple location was the effect of radiation on the thermocouple measurement. A thermal model was developed to aid in characterization of the path of heat transfer from the reaction to the thermocouple. It was found that the radiation heat transfer from the platinum catalyzed surface reaction was negligible compared to the convective heat transfer of the hot gases flowing over the thermocouple bead.

Flow rate considerations were of importance in this investigation as well. When first running the experiment, it was found that the size and temperature of the reaction zone significantly affected the flow stability. When combustion was attained, the temperature of the combustion region would significantly increase, causing an increase in pressure in the upstream section, which would in turn cause a change in the volumetric flow rate and mixture composition. Mass flow controllers were used because they regulate flow on a mass basis, thus nullifying the varying effects of temperature and pressure on the propane/air mixture. Inserting mass flow controllers into the air and fuel lines allowed for variation of inline pressure while maintaining consistent mixture flow rates. All measurements were collected with the mass flow controllers in place.

4.5 Experimental Results and Discussion

A picture of the catalytic reaction can be seen in Fig. 4.3. The exothermic reactions are shown to be taking place on the surface of the platinum coil. The thermocouple can be seen just to the left of the glowing coil. The brightness of the surface reaction was found to be directly proportional to the fuel flow rate and dependent on the stoichiometric mixture ratio.

The results of the first test are presented in Fig. 4.4. The data show an increase in reaction temperature with increasing fuel flow rate. This increase however does not appear to be linear, but rather to asymptotically approach some maximum temperature at higher fuel flow rates. This may be caused by an increase in convective heat loss and decreasing diffusion of active species to the platinum surface as mixture flow rates increase. Also shown in the graph is an inverted U-shape trend indicating a maximum reaction temperature exists. This maximum temperature occurs at slightly rich mixtures. The surface area of the platinum coil, the amount of oxidation and corrosion damage in the system, and the location of the

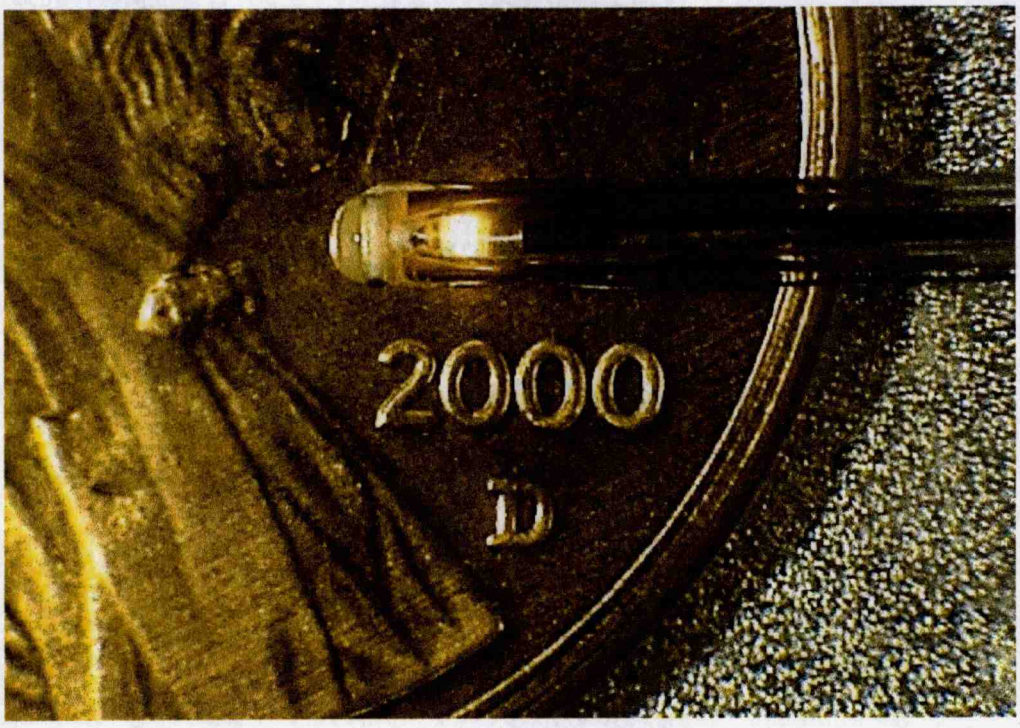

Figure 4.3. Platinum catalytic reaction with propane

thermocouple with respect to the reaction zone directly influence the measured maximum temperature of the microcombustor. The results also show a decrease in combustion temperature and flame stability toward the flammability limits.

The results of the second set of experiments are seen in Fig. 4.5. This set of data shows the same trends as in the first set. There are differences in the temperature values up to 150°C at the maximum reaction temperature. This is believed to be due to two conditions. First, there was a significant amount of corrosion damage built-up in the first test system. Second, due to the size of this chamber, it was not possible to recreate the first test set-up exactly. For example, the number of coils may have varied slightly. This would change the surface area on which the reaction could take place. Also the thermocouple appeared to be slightly closer to the platinum coil in the second system. In the second test, rich and lean mixtures were varied until combustion was no longer attained or the limits of the flow controllers were reached. This increased the range of data and further indicated limits of

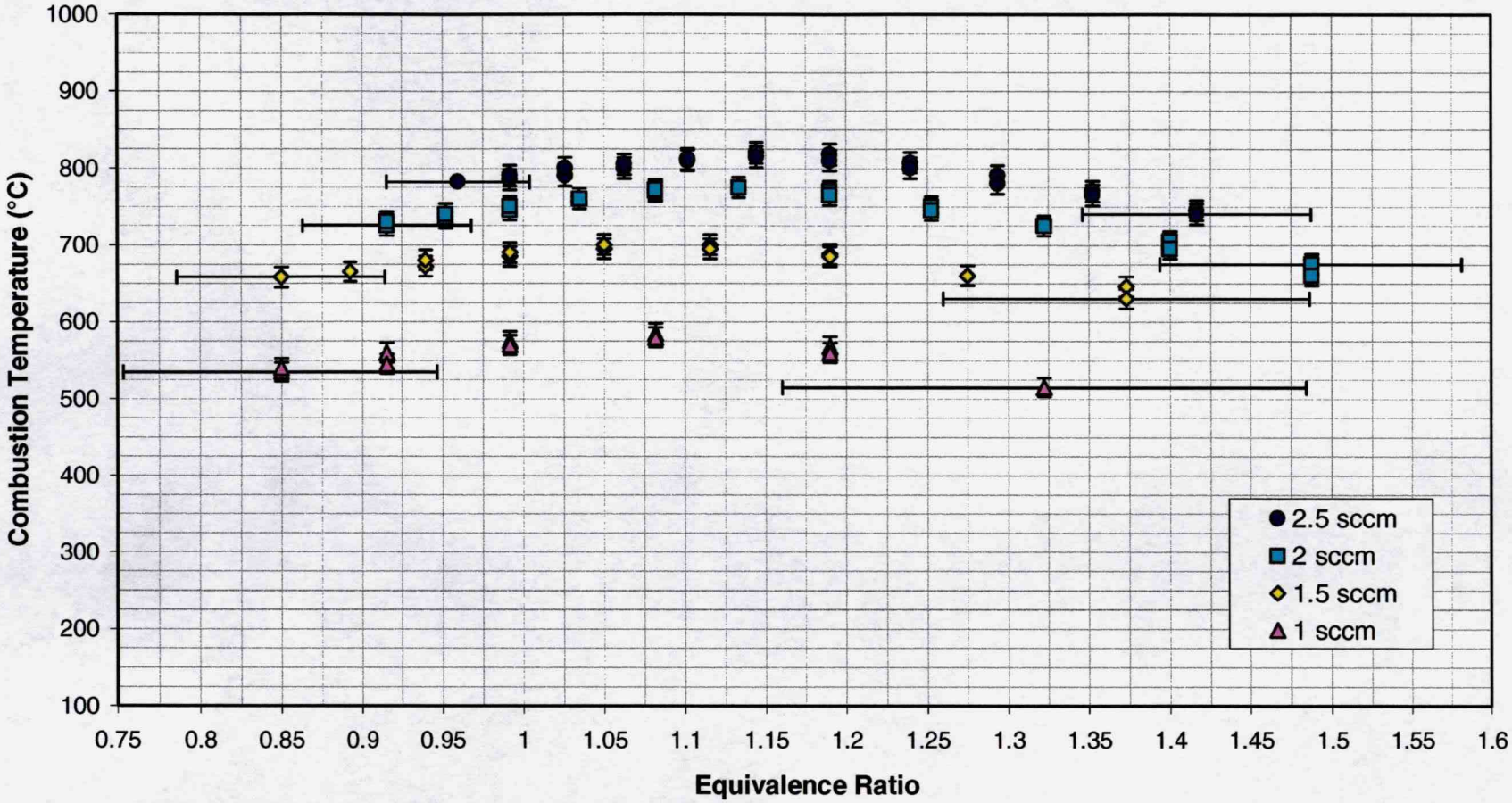

Figure 4.4. Results from the first microcombustor test

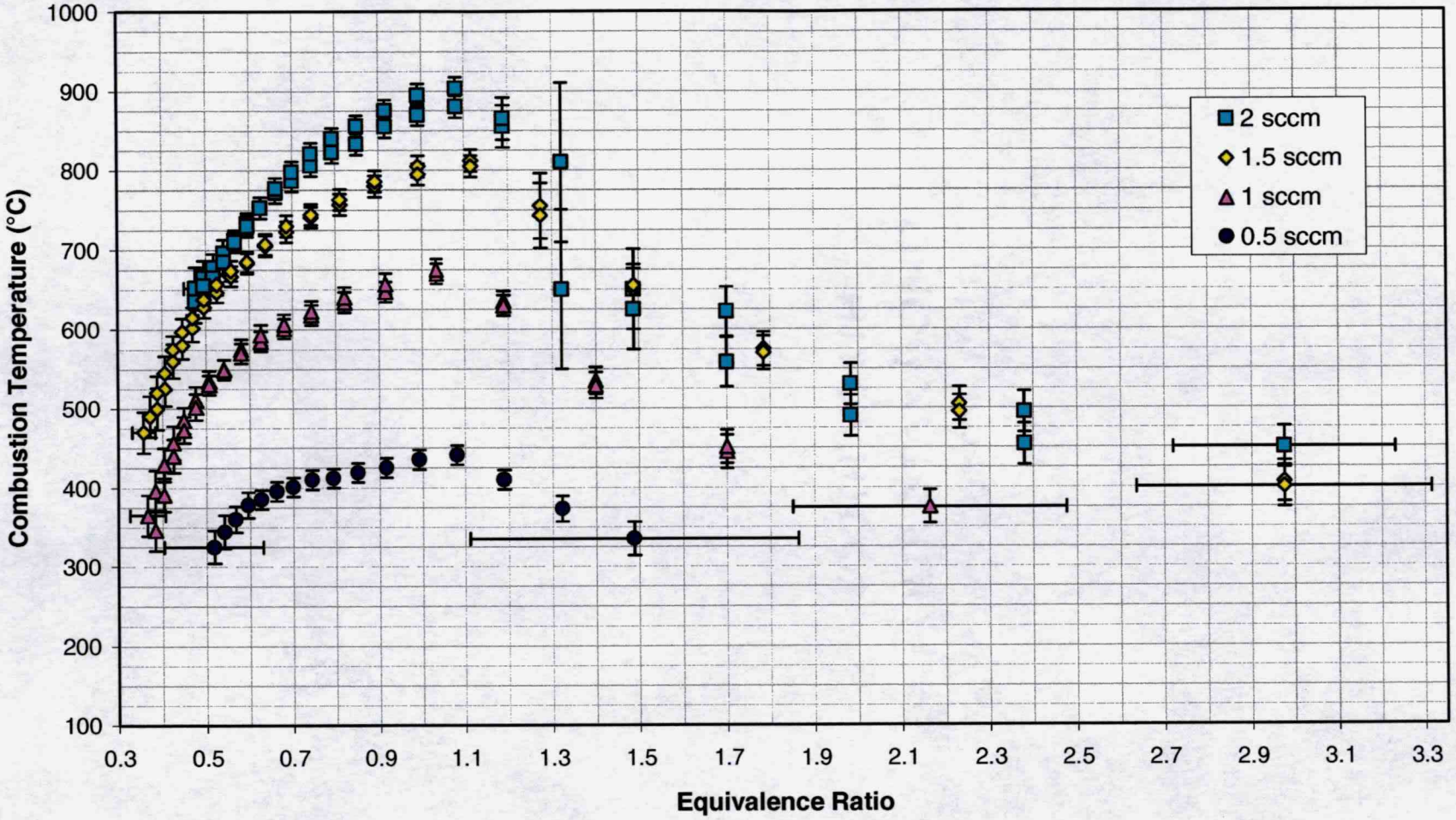

Figure 4.5. Results from the second microcombustor test

flammability. The measured temperature data indicates an increase in flammability limits as the fuel flow rate is increased.

Figure 4.6 shows calculations of heat release based on the fuel flow rates examined in this experiment burned with a stoichiometric amount of air. The volume of the combustion chamber can be approximated by a cylinder 0.6 mm in diameter and between ¾ and 1 mm in length. This gives a combustion chamber of volume ~ 0.25 mm^3. From this information, an indication is given of the rate at which energy can be released per combustor volume for the microcombustor setup.

Fuel Flow Rate (sccm)	Air Flow Rate (sccm)	Heat Release (W)
0.5	1.28	0.09
1.0	2.56	0.19
1.5	3.84	0.28
2.0	5.13	0.37
2.5	6.41	0.46

Figure 4.6. Heat release of propane at stoichiometric conditions

Some interesting observations were made while testing the second microcombustor assembly. For higher fuel flow rates, the uncertainty in the measurements on the rich side significantly increased. For example, for a fuel flow rate of 2 sccm, the temperature measurement began to oscillate at ±100°C at an equivalence ratio of 1.3. This oscillation was also observed in the 1.5 sccm fuel flow data, but not as pronounced. The oscillations were more pronounced at 2.5 sccm in the second test and made data collection impossible. These oscillations were coincident with a visible change in location of the reaction along the coil. As the system would oscillate the reaction appeared to work its way from the platinum coil down the stainless steel tube and then back again. At even richer mixtures, the oscillations were much slower and smaller in amplitude.

Insulative effects of the quartz tubing as described above were also reflected in this test system. Blowing on the quartz envelope caused a decrease in the reaction temperature and subsequently a decrease in the brightness of the surface reaction. This is consistent with the notion that increasing the convective heat transfer from the quartz tube decreases the inner tube wall temperature and increases heat loss from the reaction zone.

4.6 Uncertainty Analysis

Uncertainty was calculated for this experiment using the Kline-McClintock[14] method. In this analysis, all sources of uncertainty are combined to indicate total uncertainty in a quantity. In this set of experiments, measured temperature and mixture composition require estimations of uncertainty.

The uncertainty in the temperature measurements was calculated using the same analysis as in the previous section. The main difference between this test and the previous was that of thermocouple location. In this set of tests, the goal was not to measure a wall temperature, but to measure a temperature of the reaction zone. The before mentioned thermal model was used to show that the radiation from the flame had no significant effect compared to that of convection due to the exhaust gases flowing over the thermocouple. The thermal model also showed that the response time of the thermocouple was sufficiently low. The major contributor to uncertainty in the experiment was determined to be the repeatability of the temperature measurements. At higher temperatures, the uncertainty in the thermocouple also played a significant role. The values of uncertainty ranged from ±12°C at stoichiometric mixtures to ±30°C at rich and lean mixture limits. Uncertainty in the oscillatory data was estimated to reach ±100°C for higher flow rates.

The uncertainty in the reactant mixture ratio was significantly different in this set of experiments due to the use of mass flow controllers. The mass flow controllers were selected such that there full-scale range was just large enough to handle the desired flow rates. This was done to reduce the percentage uncertainty in the mixture composition. Because uncertainty of these devices was specified as a percentage of full scale, the same absolute uncertainty was attributed at each mixture flow rate. As result, at low flow rates the uncertainty in the mixture ratio reached ±25%, while at high flow rates the mixture ratio uncertainty approached ±5%. This proved to be the major contributing factor in the uncertainty attributed to mixture composition. Uncertainty of the equivalence ratio was calculated to be ±0.30 for low mixture flow rates and ±0.03 for high mixture rates.

5 CONCLUDING REMARKS

In this research, two test systems were developed to aid in the prediction of reaction behavior for microscale combustion. The first included measurements of wall temperature coincident with a propagating flame front for various hydrocarbon fuels and system configurations. Wall temperature was plotted against tube diameter. Results demonstrated that as the tube diameter decreases, the required wall temperature to propagate a flame increases. Tube diameters ranged between 0.8 mm and 2.2 mm. The second involved miniaturization of a catalytic combustor and a measurement of the reaction zone temperature. Reaction temperature was plotted against equivalence ratio for a propane/air mixture and a 0.25 mm^3 quartz chamber using platinum as a catalyst. Results showed that a self-sustaining surface catalyzed reaction could be attained in the microscale regime and that reaction temperatures ranged from 400 to 900°C depending on the mixture flow rate.

There are a few factors that appear to affect combustion at the microscale level. The first set of experiments dealt primarily with the thermal aspect of quenching. The second set of experiments employed a scheme designed to reduce quenching from deactivation of species. It is believed that this aspect will play an increasingly important role in the future as combustor size is further reduced. More research is needed to further determine the feasibility of developing microcombustors for power generation.

REFERENCES

[1]Glassman, I. *Combustion*, 3rd Edition; Academic Press: San Diego, CA, 1996; pp 170-171.

[2]Kanury, M. A. *Introduction to Combustion Phenomena*; Gordon and Breach Science Publishers: New York, 1975; pp 99-131.

[3]Soyema, T. *Advanced Combustion Science*; Springer-Verlag: Tokyo, 1993; pp 232-233.

[4]Lucht R P and Maris M A (1987) CARS measurements of temperature profiles near a wall in an internal combustion engine, SAE Paper 870459.

[5]Zamashchikov, V. V. Combustion of Gases in Thin-Walled Small Diameter Tubes, *Combustion, Explosion, and Shock Waves*, Vol. 31, No. 1, January-February, 1995.

[6]Cooley, B. A. Exploring the Limits of Microscale Combustion. M.S. Thesis, University of California, Berkeley, CA, Spring 1999.

[7]Peterson, R. B. A Catalytic Combustor for Microscale Applications, *Combustion Science and Technology Communications*, Vol 1, July 2000.

[8]Sitzki, L., Borer, K., Wussow, S., Schuster, E., Maruta, K., Ronney, P. Combustion and Power Generation in Microscale Excess Enthalpy Burners, *2nd Joint Meeting of the US Section of the Combustion Institute*, Oakland, CA, March 26-29, 2001.

[9]Mayer,E. A Theory of Flame Propagation Limits Due to Heat Losses, *Combustion and Flame*, Vol. 1, December 1957.

[10]Williams, F. A. *Combustion Theory*; Addison-Wesley Publishing: Boston, MA, 1965; pp 187-200.

[11]Brigham Young University. Thermophysical Properties Database. http://dippr.byu.edu (accessed February 2001).

[12]*Handbook of Chemistry and Physics*, 54th Edition; Weist, R. C.; CRC Press: Cleveland, OH, 1973; pp D-76.

[13]Incropera, F.P., DeWitt, D.P. *Fundamentals of Heat and Mass Transfer*, 4th Edition; John Wiley & Sons, Inc: New York, 1996; pp 419-480.

[14]Figliola, R.S., Beasley, D.E. *Theory and Design for Mechanical Measurements*, 2nd Edition; John Wiley and Sons, Inc: New York, 1995; pp 171-217.

APPENDICES

Appendix A: Energy Potential Calculations

	Hydrogen	Propane	Hexane
Heat of Combustion (KJ/g)*	123.6	47.76	46.12
Fuel density @ STP (kg/m3)	0.09	1.86	660.37
Fuel flow rate (sccm)**	1.0	1.0	1.0
Heat Release Rate (W)* **	**0.19**	**1.48**	**507.60**

*Kanury, Murty. *Introduction to Combustion Phenomena.*
**Flow rates at standard temperature and pressure.
***Heat Release based on fuel burned with stoichiometric amount of air

Figure A.1. Calculations of heat release rate

	Energizer "AA"	Hydrogen	Propane	Hexane
Capacity (mAh)	2850			
Voltage (V)	1.5			
Weight (g)	23			
Energy Density (KJ/g)	**0.67**	**123.60***	**47.76***	**46.12***

*Based on heat of combustion

Figure A.2. Energy density comparison

Appendix B: Development of Thermal Model Estimating Unburnt Mixture Temperature

The following thermal model was used to estimate the temperature of the unburnt mixture as it entered the reaction zone. The temperature profile along the tube was assumed linear between the base, at vaporizer temperature, and the thermocouple location, at an elevated temperature. Figure B.1 shows the temperature profiles of the tube wall and fluid along the tube.

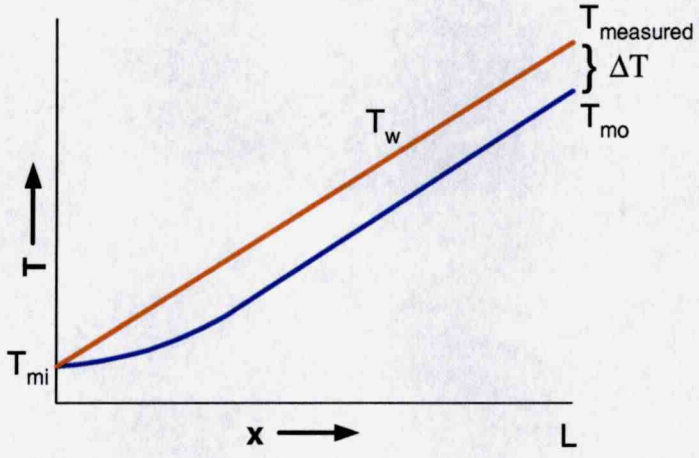

Figure B.1. Tube wall and fluid temperature profiles along the tube

The following energy transfer equations apply to laminar flow in tubes

$$q = \dot{m} \cdot c_p \cdot (T_{mo} - T_{mi})$$

$$q = \bar{h} \cdot A \cdot \Delta T = \frac{Nu \cdot \bar{k}}{d} \cdot \pi \cdot d \cdot L \cdot \Delta T = Nu \cdot \bar{k} \cdot \pi \cdot L \cdot \Delta T$$

The first equation describes the energy gained/lost by the fluid as it passes through the tube. The second equation describes the energy transferred from the tube walls to the fluid. In this analysis, a Nusselt number of 4 was used to approximate tube wall temperature effects. It was also assumed that the temperature difference between the tube wall and the mean flow was constant along the tube. Using the temperature difference between the thermocouple measurement and the desired fluid mean outlet temperature allowed the above equations to be simplified as follows

$$T_{mo} = \frac{\dot{m} \cdot c_p \cdot T_{mi} + Nu \cdot \bar{k} \cdot \pi \cdot L \cdot T_{measured}}{\dot{m} \cdot c_p + Nu \cdot \bar{k} \cdot \pi \cdot L}$$

where T_{mi} is the temperature of the vaporizer, L is the length of the tube between the vaporizer and the thermocouple location, and $T_{measured}$ is the quench temperature.

Appendix C: Quench Test Data

Vaporizer temp	RT		
fuel density (kg/cm^3)	0.00000183		
air density (kg/cm^3)	0.00000118		
mass a/f	15.63		
ID (mm)	0.8		
air flow (mL/sec)	0.175		
Fuel (mL/min)	**Temp (°C)**	**mass a/f**	**Eq Ratio**
0.45	914.00	14.87	1.05
0.5	891.30	13.38	1.17
0.55	892.00	12.17	1.28
0.6	900.03	11.15	1.40
0.65	915.65	10.29	1.52
0.7	952.65	9.56	1.64
0.75	1006.40	8.92	1.75
ID (mm)	1.1		
air flow (mL/sec)	0.3		
Fuel (mL/min)	**Temp (°C)**	**mass a/f**	**Eq Ratio**
0.65	823.30	17.58	0.89
0.7	802.00	16.32	0.96
0.75	784.77	15.23	1.03
0.8	774.20	14.28	1.09
0.85	769.88	13.44	1.16
0.9	758.54	12.70	1.23
0.95	768.46	12.03	1.30
1	779.00	11.43	1.37
1.05	803.15	10.88	1.44
air flow (mL/sec)	0.22		
Fuel (mL/min)	**Temp (°C)**	**mass a/f**	**Eq Ratio**
0.5	760.77	16.80	0.93
0.55	746.00	15.27	1.02
0.6	733.40	14.00	1.12
0.65	727.03	12.92	1.21
0.7	731.50	12.00	1.30
0.75	745.50	11.20	1.40
0.8	779.20	10.50	1.49
ID (mm)	1.95		
air flow (mL/sec)	0.51		
Fuel (mL/min)	**Temp (°C)**	**mass a/f**	**Eq Ratio**
1.1	558.38	17.43	0.90
1.2	499.95	15.98	0.98
1.35	441.51	14.20	1.10
1.425	433.38	13.46	1.16
1.5	428.44	12.78	1.22
1.575	435.25	12.18	1.28
1.65	464.06	11.62	1.34
1.725	501.88	11.12	1.41
1.8	557.25	10.65	1.47
air flow (mL/sec)	0.375		
Fuel (mL/min)	**Temp (°C)**	**mass a/f**	**Eq Ratio**
0.8	484.00	17.72	0.88
0.9	429.00	15.75	0.99
1	392.45	14.17	1.10
1.1	370.30	12.88	1.21
1.2	406.75	11.81	1.32
1.3	474.00	10.90	1.43
1.4	583.00	10.12	1.54

Figure C.1. Propane quench test data

vaporizer temp	80°C		
fuel density (kg/cm^3)	0.000659		
air density (kg/cm^3)	0.00000118		
mass a/f	15.202		
ID (mm)	0.8		
air flow (mL/sec)	0.22		
Fuel (mL/min)	**Temp (°C)**	**mass a/f**	**Eq Ratio**
0.0016	909.83	14.77	1.03
0.0017	894.50	13.90	1.09
0.0018	884.56	13.13	1.16
0.0019	881.50	12.44	1.22
0.002	877.67	11.82	1.29
0.0021	887.39	11.26	1.35
0.0022	911.50	10.74	1.41
ID (mm)	1.1		
air flow (mL/sec)	0.28		
Fuel (mL/min)	**Temp (°C)**	**mass a/f**	**Eq Ratio**
0.002	785.58	15.04	1.01
0.00225	774.71	13.37	1.14
0.0025	760.71	12.03	1.26
0.002625	777.38	11.46	1.33
0.00275	806.88	10.94	1.39
air flow (mL/sec)	0.39		
Fuel (mL/min)	**Temp (°C)**	**mass a/f**	**Eq Ratio**
0.00275	834.44	15.24	1.00
0.003	824.79	13.97	1.09
0.00325	820.78	12.89	1.18
0.0035	815.58	11.97	1.27
0.00375	821.22	11.17	1.36
0.004	845.75	10.47	1.45
ID (mm)	1.95		
air flow (mL/sec)	0.39		
Fuel (mL/min)	**Temp (°C)**	**mass a/f**	**Eq Ratio**
0.0025	510.83	16.76	0.91
0.003	419.70	13.97	1.09
0.0035	389.60	11.97	1.27
0.004	416.25	10.47	1.45
0.0045	551.67	9.31	1.63
air flow (mL/sec)	0.57		
Fuel (mL/min)	**Temp (°C)**	**mass a/f**	**Eq Ratio**
0.004	563.78	15.31	0.99
0.0045	519.97	13.61	1.12
0.005	485.02	12.25	1.24
0.0055	476.33	11.13	1.37
0.00575	512.33	10.65	1.43
0.006	557.28	10.21	1.49

Figure C.2. Hexane quench test data

Vaporizer Temp	240 °C		
fuel density (kg/cm^3)	0.0008		
air density (kg/cm^3)	0.00000118		
mass a/f	11.8		
ID (mm)	0.8		
air flow (mL/sec)	0.15		
Fuel (mL/min)	**Temp (°C)**	**mass a/f**	**Eq Ratio**
0.0006	845.00	22.13	0.53
0.001	843.00	13.28	0.89
0.0014	840.00	9.48	1.24
0.0018	855.00	7.38	1.60
ID (mm)	1.1		
air flow (mL/sec)	0.25		
Fuel (mL/min)	**Temp (°C)**	**mass a/f**	**Eq Ratio**
0.001	771.00	22.13	0.53
0.0012	732.50	18.44	0.64
0.0014	721.67	15.80	0.75
0.0016	701.50	13.83	0.85
0.0018	693.00	12.29	0.96
0.002	692.50	11.06	1.07
0.0022	711.67	10.06	1.17
0.0024	721.00	9.22	1.28
0.0026	780.00	8.51	1.39
air flow (mL/sec)	0.18		
Fuel (mL/min)	**Temp (°C)**	**mass a/f**	**Eq Ratio**
0.0008	732.50	19.91	0.59
0.001	681.00	15.93	0.74
0.0012	664.00	13.28	0.89
0.0014	656.00	11.38	1.04
0.0016	680.00	9.96	1.19
0.0018	744.00	8.85	1.33
ID (mm)	1.95		
air flow (mL/sec)	0.74		
Fuel (mL/min)	**Temp (°C)**	**mass a/f**	**Eq Ratio**
0.005	640.00	13.10	0.90
0.0055	569.33	11.91	0.99
0.006	547.33	10.92	1.08
0.0065	545.00	10.08	1.17
0.007	550.67	9.36	1.26
0.0075	597.67	8.73	1.35
0.008	658.33	8.19	1.44
air flow (mL/sec)	0.58		
Fuel (mL/min)	**Temp (°C)**	**mass a/f**	**Eq Ratio**
0.004	525.00	12.83	0.92
0.0045	475.00	11.41	1.03
0.005	460.00	10.27	1.15
0.0055	450.00	9.33	1.26
0.006	465.00	8.56	1.38
0.0065	550.00	7.90	1.49

Figure C.3. Kerosene quench test data

Vaporizer Temp	240 °C		
fuel density (kg/cm^3)	0.00092		
air density (kg/cm^3)	0.00000118		
mass a/f	14.98		
ID (mm)	0.8		
air flow (mL/sec)	0.18		
Fuel (mL/min)	**Temp (°C)**	**mass a/f**	**Eq Ratio**
0.0026	846.00	5.33	2.81
0.003	850.00	4.62	3.24
0.0034	850.00	4.07	3.68
0.0038	850.00	3.65	4.11
0.0042	847.00	3.30	4.54
ID (mm)	1.1		
air flow (mL/sec)	0.29		
Fuel (mL/min)	**Temp (°C)**	**mass a/f**	**Eq Ratio**
0.0024	760.00	9.30	1.61
0.0027	743.50	8.27	1.81
0.003	732.00	7.44	2.01
0.0033	737.50	6.76	2.22
0.0036	742.00	6.20	2.42
0.0039	745.00	5.72	2.62
0.0042	750.50	5.31	2.82
0.0045	760.00	4.96	3.02
air flow (mL/sec)	0.22		
Fuel (mL/min)	**Temp (°C)**	**mass a/f**	**Eq Ratio**
0.0018	745.00	9.41	1.59
0.0021	709.00	8.06	1.86
0.0024	693.50	7.05	2.12
0.0027	695.50	6.27	2.39
0.003	701.00	5.64	2.65
0.0033	705.50	5.13	2.92
0.0036	745.00	4.70	3.19
ID (mm)	1.95		
air flow (mL/sec)	0.93		
Fuel (mL/min)	**Temp (°C)**	**mass a/f**	**Eq Ratio**
0.008	655.00	8.95	1.67
0.009	620.50	7.95	1.88
0.01	598.00	7.16	2.09
0.011	584.50	6.51	2.30
0.012	588.00	5.96	2.51
0.013	591.50	5.51	2.72
0.014	595.50	5.11	2.93
0.015	633.00	4.77	3.14
0.016	660.00	4.47	3.35
air flow (mL/sec)	0.74		
Fuel (mL/min)	**Temp (°C)**	**mass a/f**	**Eq Ratio**
0.007	545.50	8.14	1.84
0.008	503.50	7.12	2.10
0.009	480.50	6.33	2.37
0.01	480.50	5.69	2.63
0.011	491.00	5.18	2.89
0.012	506.00	4.75	3.16
0.013	546.00	4.38	3.42

Figure C.4. Diesel quench test data

Appendix D: Calculations of Quench Temperature and Flame Temperature

Diameter (mm)	0.8	1.1	1.1	1.95	1.95	2.2
mass flow rate (kg/s)	2.22E-07	3.80E-07	2.78E-07	6.45E-07	4.74E-07	1.39E-06
specific heat fluid (J/kg K)	1.27E+03	1.23E+03	1.22E+03	1.14E+03	1.13E+03	1.11E+03
Nusselt	4	4	4	4	4	4
conductivity fluid (W/m K)	5.45E-02	5.01E-02	4.93E-02	3.81E-02	3.67E-02	3.46E-02
tube length (m)	0.02	0.02	0.02	0.02	0.02	0.02
Tvaporizer (K)	298	298	298	298	298	298
Tmeasured (K)	1150	1030	1000	690	640	610
Tadflame (K)	2400	2400	2400	2400	2400	2400
Tunburnt (K)	1133	1004	981	662	621	563
Tunburnt (K) theory	1133	1004	981	662	621	563
flame speed (m/s)	1.3930119	1.1167417	0.7996059	0.3979572	0.2744587	0.574864
specific heat unburnt (J/kg K)	1.47E+03	1.42E+03	1.41E+03	1.24E+03	1.21E+03	1.18E+03
density unburnt (kg/m3)	3.17E-01	3.58E-01	3.66E-01	5.43E-01	5.78E-01	6.38E-01
density ave (kg/m3)	2.26E-01	2.36E-01	2.38E-01	2.66E-01	2.70E-01	2.76E-01
conductivity ave (W/m K)	1.10E-01	1.06E-01	1.06E-01	9.58E-02	9.45E-02	9.27E-02
Tflame (K)	2040	2040	2040	2040	2040	2040
Twall (K) theory	1681	1527	2040	1714	2040	1011
flame speed (m/s)	1.3930119	1.1167417	0.7996059	0.3979572	0.2744587	0.574864
specific heat unburnt (J/kg K)	1.47E+03	1.42E+03	1.41E+03	1.24E+03	1.21E+03	1.18E+03
density unburnt (kg/m3)	3.17E-01	3.58E-01	3.66E-01	5.43E-01	5.78E-01	6.38E-01
density ave (kg/m3)	2.42E-01	2.49E-01	2.67E-01	3.08E-01	3.43E-01	2.84E-01
conductivity ave (W/m K)	1.04E-01	1.01E-01	9.54E-02	8.43E-02	7.65E-02	9.03E-02
Tflame (K) guess	1830	1881	1710	1673	1471	1963
Tflame (K) theory	1830	1882	1711	1674	1472	1964

Figure D.1. Quench test calculations for propane

Diameter (mm)	0.8	1.1	1.1	1.95	1.95
mass flow rate (kg/s)	7.049E-08	1.009E-07	1.328E-07	2.194E-07	2.814E-07
specific heat fluid (J/kg K)	1291.8176	1255.7945	1272.6473	1150.523	1176.3961
Nusselt	4	4	4	4	4
conductivity fluid (W/m K)	0.0552374	0.0510857	0.0530197	0.0388818	0.0419493
tube length (m)	0.02	0.02	0.02	0.02	0.02
Tvaporizer (K)	350	350	350	350	350
Tmeasured (K)	1150	1025	1086	660	755
Tadflame (K)	2400	2400	2400	2400	2400
Tunburnt (K)	1145	1018	1077	652	743
Tunburnt (K) theory	1145	1018	1077	652	743
flame speed (m/s)	1.432043	0.8570914	1.262996	0.2432992	0.4052285
specific heat unburnt (J/kg K)	1.42E+03	1.38E+03	1.40E+03	1.22E+03	1.27E+03
density unburnt (kg/m3)	3.20E-01	3.60E-01	3.41E-01	5.63E-01	4.94E-01
density ave (kg/m3)	2.30E-01	2.40E-01	2.35E-01	2.73E-01	2.64E-01
conductivity ave (W/m K)	1.06E-01	1.03E-01	1.05E-01	9.23E-02	9.49E-02
Tflame (K)	2040	2040	2040	2040	2040
Twall (K) theory	1654	1727	1415	1905	1715
flame speed (m/s)	1.432043	0.8570914	1.262996	0.2432992	0.4052285
specific heat unburnt (J/kg K)	1.42E+03	1.38E+03	1.40E+03	1.22E+03	1.27E+03
density unburnt (kg/m3)	3.20E-01	3.60E-01	3.41E-01	5.63E-01	4.94E-01
density ave (kg/m3)	2.45E-01	2.65E-01	2.43E-01	3.54E-01	3.02E-01
conductivity ave (W/m K)	1.01E-01	9.46E-02	1.02E-01	7.35E-02	8.45E-02
Tflame (K) guess	1848	1755	1945	1418	1686
Tflame (K) theory	1848	1755	1945	1418	1687

Figure D.2. Quench test calculations for hexane

Appendix E: Microcombustor Test Data

Air Flow (sccm)	Fuel Flow (sccm)	Temperature #1 (°C)	Temperature #2 (°C)	Equivalence Ratio
18	1	515	515	1.32
20	1	568	560	1.19
22	1	585	580	1.08
24	1	575	570	0.99
26	1	560	545	0.92
28	1	535	540	0.85
26	1.5	646	630	1.37
28	1.5	660	660	1.28
30	1.5	688	685	1.19
32	1.5	700	695	1.12
34	1.5	695	700	1.05
36	1.5	685	690	0.99
38	1.5	672	680	0.94
40	1.5	665	665	0.89
42	1.5		658	0.85
32	2	675	660	1.49
34	2	705	695	1.40
36	2	725	725	1.32
38	2	750	745	1.25
40	2	770	765	1.19
42	2	775	775	1.13
44	2	770	772	1.08
46	2	760	760	1.03
48	2	745	750	0.99
50	2	735	740	0.95
52	2	725	730	0.92
42	2.5	745	740	1.42
44	2.5	770	765	1.35
46	2.5	790	780	1.29
48	2.5	807	800	1.24
50	2.5	818	810	1.19
52	2.5	820	815	1.14
54	2.5	810	812	1.10
56	2.5	800	805	1.06
58	2.5	790	800	1.03
60	2.5	785	790	0.99
62	2.5		782	0.96

Figure E.1. First microcombustor test data

Air Flow (sccm)	Fuel Flow (sccm)	Temperature #1 (°C)	Temperature #2 (°C)	Equivalence Ratio
8	0.5		335	1.49
9	0.5		373	1.32
10	0.5		410	1.19
11	0.5		441	1.08
12	0.5		435	0.99
13	0.5		425	0.92
14	0.5		419	0.85
15	0.5		412	0.79
16	0.5		410	0.74
17	0.5		401	0.70
18	0.5		395	0.66
19	0.5		385	0.63
20	0.5		378	0.60
21	0.5		360	0.57
22	0.5		344	0.54
23	0.5		325	0.52
11	1		375	2.16
14	1	445	451	1.70
17	1	535	529	1.40
20	1	635	630	1.19
23	1	670	675	1.03
26	1	647	657	0.92
29	1	634	640	0.82
32	1	618	623	0.74
35	1	601	606	0.68
38	1	585	593	0.63
41	1	575	570	0.58
44	1	550	549	0.54
47	1	535	530	0.51
50	1	511	502	0.48
53	1	485	473	0.45
56	1	457	440	0.43
59	1	429	391	0.40
62	1	396	346	0.38
65	1	365		0.37

Figure E.2. Second microcombustor test data

Air Flow (sccm)	Fuel Flow (sccm)	Temperature #1 (°C)	Temperature #2 (°C)	Equivalence Ratio
12	1.5	406	400	2.98
16	1.5	505	495	2.23
20	1.5	575	570	1.79
24	1.5	650	655	1.49
28	1.5	755	743	1.28
32	1.5	812	805	1.12
36	1.5	805	795	0.99
40	1.5	780	786	0.89
44	1.5	757	763	0.81
48	1.5	741	744	0.74
52	1.5	723	730	0.69
56	1.5	705	707	0.64
60	1.5	683	685	0.60
64	1.5	667	674	0.56
68	1.5	647	657	0.53
72	1.5	628	638	0.50
76	1.5	602	615	0.47
80	1.5	580	597	0.45
84	1.5	560	575	0.43
88	1.5	525	545	0.41
92	1.5	500	520	0.39
96	1.5		490	0.37
100	1.5		470	0.36
16	2	450		2.98
20	2	495	454	2.38
24	2	530	490	1.98
28	2	558	622	1.70
32	2	650	625	1.49
36	2	810	650	1.32
40	2	855	865	1.19
44	2	880	903	1.08
48	2	870	895	0.99
52	2	855	875	0.92
56	2	833	856	0.85
60	2	823	840	0.79
64	2	806	821	0.74
68	2	787	798	0.70
72	2	772	777	0.66
76	2	753	753	0.63
80	2	733	730	0.60
84	2	712	710	0.57
88	2	696	685	0.54
92	2	678	665	0.52
96	2	665	655	0.50
100	2	652	635	0.48

Figure E.3. Second microcombustor test data (cont.)